Deciphering the origin of the Cenozoic intracontinental rifting and volcanism in eastern China using integrated evidence from the Jianghan Basin

Lulu Wu [a], Lianfu Mei [a*], Douglas A. Paton [b], Pengyuan Guo [c], Yunsheng Liu [d], Jin Luo [d], Deliang Wang [a], Minghua Li [d], Peng Zhang [a], Hui Wen [d]

[a] Key Laboratory of Tectonics and Petroleum Resources, Ministry of Education, China University of Geosciences, Wuhan 430074, China

[b] Basin Structure Group, School of Earth and Environment, University of Leeds, Leeds, LS2 9JT, UK

[c] Institute of Oceanology, Chinese Academy of Sciences, Qingdao 266071, China

[d] Research Institute of Exploration and Development, Jianghan Oilfield Branch Company, SINOPEC, Wuhan 430223, China

*Corresponding author: Lianfu Mei, E-mail: lfmei@cug.edu.cn

Abstract

Intracontinental rifting and low-volume volcanism are a globally common phenomenon, yet the underlying driving mechanisms and whether they can be explained through classic plate tectonic concepts, remain hotly debated. A prominent example is the Cenozoic rift and volcanic province in eastern China. Using an integration of geological, geophysical and geochemical data, we unravel the spatial and temporal variations of the rifting and volcanism in the Jianghan Basin. Both rifting and volcanism in the Jianghan Basin show two intense-to-weak cycles (65-50 Ma and 50-26 Ma, respectively) with significant enhancement in activity during the late rift phase. Moreover, rifting and depocentres progressively migrated eastward. The Jianghan basalts all share an asthenospheric origin while the source of the late phase basalts is slightly more enriched and heterogenous in Nd-Hf isotopes than that of the early phase basalts. The late phase basalts also display a smaller extent of partial melting even under a thinner lithosphere, likely indicating a significant decrease of volatile content in the mantle source. Based on regional tectonic correlations, the main stages of tectonic evolution of the Jianghan Basin and eastern China are not synchronous with changes in Pacific plate motion, while they are coincident with India-Asia collision processes. These observations lead us to propose that the asthenospheric flow driven by India-Asia collision rather than the rollback of the subducted Pacific slab has caused the widespread rifting and volcanism in eastern China. The variations of rifting and volcanism in the Jianghan Basin suggest a multiphase and eastward asthenospheric flow beneath eastern China driven by India-Asia collision, with an intense upwelling when passing through the North-South Gravity Lineament (NSGL). The much more intense rifting and volcanism during the late rift phase may indicate a much larger scale of volatile-poor asthenospheric flow than the early rift phase which could result in a more intense erosion of ancient enriched lithospheric mantle and the volatile content in the mantle source dropping sharply. This study provides an improved model based on our multidisciplinary observations for asthenospheric flow which may be an alternative driving mechanism for intracontinental rifting and low-volume volcanism in the regions where there are step changes in lithospheric thickness globally.

Keywords: Intracontinental rifting; Intracontinental volcanism; Asthenospheric flow; Jianghan Basin; Eastern China.

1. Introduction

Intracontinental rifting and volcanism are often coupled and form extensive rift and volcanic provinces, such as the Basin and Range Province, Carpathian-Pannonian region and Baikal Rift area (e.g., Putirka and Platt, 2012; Harangi, et al., 2015; Ivanov et al., 2015). While some studies attribute the development of these rift and volcanic systems to plate boundary processes and classic lithospheric stretching models (e.g., Baikal Rift, Petit and Deverchere, 2006; eastern China, Xu et al., 2012; Niu, 2013), this is highly controversial as these provinces are often away from plate boundaries and typically involve widely dispersed, low volume volcanism (Conrad et al., 2011; Davies and Rawlinson, 2014) compared to the large igneous provinces (Bryan and Ferrari, 2013) . As a consequence, some studies argued that these classical models are either not appropriate, or require modification, and invoke a range of other processes, such as flat-slab rollback (e.g., the Cretaceous South China Block, Li et al., 2012b, 2014; Basin and Range Province, Porter et al., 2014), sub-horizontal asthenospheric flow (e.g., Baikal Rift, Lebedev et al., 2006; Pannonian Basin, Harangi, et al., 2015; eastern China, Liu et al., 2004; Niu, 2005) and edge-driven convection (e.g., Newer Volcanics Province, Davies and Rawlinson, 2014). This ambiguity is compounded by the need to have a comprehensive analysis of geological, geophysical and geochemical data, and the incomplete suite of such data in many studies, resulting in the driving forces varying not only from one province to another, but often within the same province or even in the same area.

The Cenozoic eastern China characterized by widespread rift basins and basalts (Figs. 1 and 2A) typifies the debate on the genesis and processes of intracontinental rifting and volcanism. Although extensive research has focused on the origin of the widespread Cenozoic rifting and volcanism in eastern China (e.g., Flower et al., 2001; Ren et al., 2002; Liu et al., 2004; Niu, 2005; Tang et al., 2006; Xu, 2007; Li et al., 2010, 2013, 2015b, 2016b; Yin, 2010; Zhao et al., 2011; Xu et al., 2012; Suo et al., 2012, 2014; Kuritani et al., 2013; Sakuyama et al., 2013; Gong and Chen, 2014; Wang et al., 2015; Zhao et al., 2016; Chen et al., 2017; Sun et al., 2017), controversy remains and two alternative models are currently invoked. These two competing models have evoked fundamentally different lithospheric and asthenospheric processes as they involve different driving forces (Fig. 2B and C). The passive rifting and upwelling model states that the retreat of subduction zone causes the lithosphere of eastern China to extend (Niu, 2013), inducing asthenospheric mantle to upwell and melt (Xu et al., 2012; Li et al., 2015b). Therefore, its driving force is the rollback of the subducted Pacific slab (Niu, 2013). On the contrary, the active rifting and upwelling model suggests that the India-Asia collision has induced an eastward asthenospheric flow beneath eastern China and the eastward asthenospheric flow experience an upwelling and decompression when flowing through the North-South Gravity Lineament (NSGL) (Niu, 2005; Sun et al., 2017), causing the lithosphere of eastern China to extend and the flowing asthenospheric mantle to melt (Liu et al., 2004).

In this study, for the first time, we apply a multidisciplinary approach (including 2-D and 3-D seismic reflection data, borehole data, field data and geochemical data) to investigate the temporal and spatial variations of rifting and volcanism in the Jianghan Basin, eastern China. Our quantitative study of shallow physical and chemical changes throughout the Cenozoic, including fault and volcanic activity and geochemical compositions of basalts, can release abundant information about deep physical and chemical processes and mantle dynamics. Furthermore, we consider the evolution of the Jianghan Basin within a regional context and make tectonic correlations between them. Our findings not only address the relative role of pacific plate subduction and India-Asia collision on regional geodynamics, but also provide invaluable insights into the origin of intracontinental rifting and low-volume volcanism that often remain enigmatic globally.

2. Geological setting

The western boundary of eastern China is approximately defined by the north-south trending NSGL (Figs. 1, 2A). The NSGL is not only an evident gravity lineament, but also displays a major transition of elevation, topography, crustal and lithospheric thickness (Niu, 2005). Furthermore, it is broadly coincident with the western edge of the stagnant Pacific slab which is presently lying horizontally in the mantle transition zone (MTZ; Huang and Zhao, 2006). The Jianghan Basin is located on the north margin of the South China Block (SCB) and close to the NSGL (Fig. 2A), with an area of ca. 27,000 km^2. It consists of two domains (Fig. 3A): West Jianghan Basin and East Jianghan Basin. The West Jianghan Basin is predominantly controlled by the Wen'ansi Fault, Wancheng Fault and the Zibei Fault Zone, forming a large and a minor depocenters. The East Jianghan Basin consists of a large graben and a series of half-grabens. Rifting in the Jianghan Basin initiated during the Late Cretaceous under the background of widespread extension in eastern China triggered by the rollback of the subducted Pacific slab during the Early Cretaceous

(Li et al., 2012a, 2014; Wu et al., 2018). The Cretaceous widespread rifting and magmatism in eastern China marked the ultimate destruction of the North China Craton and SCB (Li et al., 2015a; Zhu et al., 2015b). During the destruction processes, the long-term dehydration (from Triassic to Cretaceous) of the subducted Pacific slab (Niu, 2005; Windley et al., 2010; Li et al., 2012a) has been crucial in weakening the ancient enriched lithospheric mantle, resulting in a juvenile depleted lithospheric mantle forming beneath eastern China (e.g., Wu et al., 2008) and a huge difference in lithospheric thickness near the NSGL (> 150 km to west of the NSGL and ca. 80 km to east of the NSGL; Li et al., 2012a, 2015a; Zhu et al., 2015b). The Jianghan Basin experienced two-phase rifting and volcanism during the Paleogene and then failed at the end of the Paleogene (Fig. 4), depositing up to ca. 8000 m thick syn-rift sediments. These syn-rift sequences can be divided into five units, namely the Shashi Formation, Xin'gouzui Formation, Jingsha Formation, Qianjiang Formation and Jinghezhen Formation.

3. Dataset and methods

The dataset for this study includes extensive 2-D and 3-D seismic reflection data, borehole data (including stratigraphic information, descriptions of drilling cores and cuttings from well completion reports, well logs and basaltic samples) and field outcrops.

3.1 Seismic reflection and borehole data and treatment

The seismic database includes > 8000 km of 2-D seismic reflection lines and ca. 5000 km^2 3-D seismic reflection surveys (Fig. 3B). The line spacing of 2-D seismic data varies from 1 to 7 km and these 2-D surveys image to depths of 5 to 6 s two-way travel time (TWTT). The 3-D seismic reflection surveys image to depths of between 5 and 6 s TWTT and have an inline and crossline spacing of 12.5 m, 25 m or 50 m. Of particular importance for this study is the generally good quality of the imaging within the Cenozoic rift sequences. Of the more than 1600 exploration wells in the basin (partly shown in Fig. 3B), about 500 wells were used for seismic-well ties and depth-conversion using synthetic seismograms (Fig. 4). Ages for the stratigraphic horizons were mainly determined by biostratigraphic data and K-Ar and Ar-Ar ages of basalt layers (Fig. 4; HBGMR, 1990; Xu et al., 1995; Peng et al., 2006).

Fault activity is estimated by observing across-fault thickening of growth strata- within seismic data (e.g., Fig. 5A, B, C, D) and quantified using fault activity rates (Figs., 5E, S1; (Thickness of hanging wall – Thickness of footwall)/Duration, Huang and Liu, 2014; Teng et al., 2016). This study uses fault activity rates rather than expansion index in determining the growth of faults, to highlight the variations of fault activity over time. This method assumes that sedimentation rates exceed fault activity rates and fault scarps are rapidly blanked by sediment (cf. Childs et al., 2003). Furthermore, the fault activity rates are time averages and may have varied within these stages. For instance, faults have a much higher activity rate during the early Qianjiang stage than that during the late Qianjiang Stage (not shown). Time-depth conversion was used when calculating strata thickness and fault activity rates (Fig. 5F). An average time-depth relationship is determined in Fig. 5F, which generally allows us to convert thicknesses measured in milliseconds two-way travel time to metres with an ca.10% error. Fault activity rates have a large variation over time, thus they are unlikely to be affected significantly by depth conversion (e.g., Fig. 5E). As most sediments near the major faults in the Jianghan Basin have a relatively low content of shale (< 70%; e.g., Fig. 7D), the influence of sediment compaction was not considered in our study (Taylor et al., 2008). Within the basin, only a few basalts outcrop on the surface (Fig.

6) as a result of salt diapirism, and most of them are deeply buried. Basaltic eruptions are conformable contact with the upper and lower strata (Figs. 6A and B, 7). Therefore, they are often referred to as “basalt layers”. Due to the continuous subsidence during the syn-rift stage, the volcanic rocks can have been well preserved beneath post-eruption sediments, rather than undergoing erosion (Jackson, 2012). Our seismic reflection data has a frequency of 30-55 Hz. With a velocity of 5000-5500 m/s, the basalt layers should be > ca. 11 m thick to be detected and > ca. 23 m thick to be resolved (cf. Watson et al., 2017). The identifiable basaltic eruptions generally manifest as very high-amplitude anomalies that have a strata-concordant morphology and low-middle continuity (Fig. 7A, B, C). These high-amplitude reflections also have a remarkable characteristic petrophysical response in well logs (Fig. 7D), namely low gamma (20-40 API) and high resistivity (10-35 Ohm m). All these data are used in combination in our study (Fig. S2). The distribution and volume of basalts were quantified by constructing thickness maps for each stage (Fig. S3). As the data of the thicknesses of basalts is from borehole data, error increases when there are limited wells to constrain thickness. Thus, the thicknesses of the Shashi Stage basalts are not used for discussion in this study.

3.2 Samples and geochemical analysis

In addition to the nine published samples (Peng et al., 2006), nine new samples from the basalt layers interlayered in the early or late rift sequences were analyzed for this study (locations in Fig. 3B, including six wells and Balingshan outcrops; detailed sample information in Table S1, Appendix A). As there is an even temporal distribution of the eighteen samples across the two rift phases, they coincide with the rifting and volcanism evolution and capture the majority of the magmatic event. The basaltic samples all exhibit an intergranular texture (Fig. 6C) and mainly contain plagioclase (60-72%), clinopyroxene (1-20%), Fe-Ti oxides (3-12%) and few olivine (less than 1%). Generally, our samples are fresh, as only a few minerals have been partially altered to iddingsite and chlorite (3-9%).

Bulk-rock analysis measured in this study includes major and trace elements and Sr-Nd-Hf isotopes. All analyses were conducted at the State Key Laboratory of Geological Processes and Mineral Resources, China University of Geosciences (Wuhan), except that the Hf isotopic analysis was finished at the Institute of Oceanology, Chinese Academy of Sciences. The detailed analytical methods are described in Appendix B.

4. Results

4.1 Multiphase rifting

Borehole calibrated seismic data provides high resolution stratigraphic constraints for calculating fault activity rates (Fig. 4). Two seismic profiles across the Wancheng Fault and Qianbei Fault are shown in Fig. 5A, B, C, and D. These two major faults are located in the West and East Jianghan basins (Fig. 3A), respectively. The Wancheng Fault decreased sharply in fault activity rates (from ca. 345 to ca. 141 m/Myr) from the Shashi Stage (65-56 Ma) to the Xin'gouzui Stage (56-50 Ma), while the Qianbei Fault underwent slightly enhanced activity (from ca. 60 m/Myr to ca. 113 m/Myr). The Qianbei Fault had a fault activity rate of up to 576 m/Myr during the Jingsha Stage (50-45 Ma), significantly higher than the Wancheng Fault (ca. 240 m/Myr). During the Qianjiang Stage (45-32 Ma), both the Wancheng Fault and the Qianbei Fault showed decreased fault activity rates (ca. 23 m/Myr and ca. 263 m/Myr, respectively). In total, the fault activity rates of the Wancheng Fault were significantly higher than the Qianbei Fault during the early rift phase, and significantly lower than the Qianbei Fault during the late rift phase (Fig. 5E).

Fault activity rates of the major faults in the Jianghan Basin are shown in Figs. 8 and S1. During the Shashi Stage (65-56 Ma), major faults in the West Jianghan Basin had much greater fault activity rates (ca. 65-345 m/Myr) than the East Jianghan Basin (0-ca. 60 m/Myr) (Fig. S1A). Faulty activity rates in the West Jianghan Basin decreased to ca. 25-140 m/Myr during the Xin'gouzui Stage (56-50 Ma) (Fig. S1B), while they generally increased in the East Jianghan Basin (ca. 10-113 m/Myr). Faulty activity rates significantly increased during the late rift phase, especially in the East Jianghan Basin. During the Jingsha Stage (50-45 Ma), fault activity was much more intense in the East Jianghan Basin (ca. 55-576 m/Myr) than the West Jianghan Basin (ca. 44-312 m/Myr) (Fig. S1C). Fault activity decayed during the Qianjiang Stage (45-32 Ma), with 0-ca. 137 m/Myr in the West Jianghan Basin and 0-ca. 263 m/Myr in the East Jianghan Basin. Activity of most major faults ceased during the Jinghezhen Stage (32-26 Ma). Only six major faults were active with relatively low fault activity rates (ca. 15-104 m/Myr). Then, rift failed at the boundary of the Paleogene and Neogene (Fig. 4).

4.2 The distribution and volume of the Jianghan basalts

The distribution and volume of the Jianghan basalts are shown in Figs. 8 and S3. During the early rift phase, the eruptions were scattered (Fig. S3A, B). The total area of the basalts erupted during the Shashi Stage (65-56 Ma) is ca. 209 km^2, while that erupted during the Xin'gouzui Stage (56-50 Ma) decreases to ca. 144 km^2 with a maximum thickness of 168.5 m. The maximum thickness of basalts erupted during the Shashi Stage is uncertain and not considered in this study, as only limited wells penetrate the basalt layers (Fig. S2A). The distribution of the basalts erupted during the Jingsha Stage (50-45 Ma) is contiguous and covers an area of ca. 1387 km^2 (Fig. S3C).

During this short timescale, up to 353 m thick basalts erupted. Volcanism moderately weakened during the Qianjiang Stage (45-32 Ma), with an area of ca. 1041 km^2 and a maximum thickness of 239 m (Fig. S3D). Volcanism terminated during the Jinghezhen Stage (32-26 Ma) (Fig. S3E). Notably, as with fault activity, volcanic activity shows two intense-to-weak cycles during the two-phase rifting.

4.3 Bulk-rock major, trace elements and Sr-Nd-Hf isotopes

The results of the major and trace elements, and Sr-Nd-Hf isotopic analyses of the Jianghan basalts are given in Table S2-S3 (Appendix A). Samples from this study are plotted together with the Cenozoic basalts from the eastern SCB for comparison (Li et al., 2015b, 2016b; Liu et al., 2016; Chu et al., 2017; Zeng et al., 2017).

The samples of the two rift phases are mainly tholeiitic basalts, with SiO_2 ranging from 50.32 to 54.57%, and the total alkali contents (Na_2O + K_2O) ranging from 3.51 to 6.79% on a volatile-free basis (Fig. S4A; Le Bas et al., 1986). They are variably evolved ($Mg^{\#}$ = 0.54-0.62) from anticipated primary magmas (i.e., $Mg^{\#} \geq 0.72$) in equilibrium with mantle olivine. The Jianghan basalts all show negative correlations of SiO_2 with MgO (Fig. S4B), while Al_2O_3, $Fe_2O_3^T$, Cr and Ni remain nearly constant with decreasing MgO (Fig. S4C, F, G, H). CaO and CaO/Al_2O_3 of the early phase basalts do not correlate with MgO (Fig. S4D, E); however, these of the late phase samples show slight negative correlations with MgO.

Fig. 9 shows chondrite-normalized rare earth element (REE) patterns and primitive-mantle normalized multi-elements spidergram of the Jianghan basalts. As with the basalts from the eastern SCB (Li et al., 2015b, 2016b; Liu et al., 2016; Chu et al., 2017; Zeng et al., 2017), all the Jianghan basalts are characterized by OIB-like trace element patterns, being progressively more enriched in the more incompatible elements. Importantly, the late phase basalts are generally more enriched in incompatible trace elements and have higher $[La/Yb]_N$ ratios (5.50-10.29, N denotes normalization to primitive mantle) than the early phase basalts ($[La/Yb]_N$ = 3.35-4.99).

The early phase basalts display large range of the $^{87}Sr/^{86}Sr_i$ ratios (0.7041-0.7088; Fig. 10A), while their $^{143}Nd/^{144}Nd$ and $^{176}Hf/^{177}Hf$ ratios are relatively restricted with $\varepsilon_{Nd}(t)$ = 2.63-3.94 and $\varepsilon_{Hf}(t)$ = 9.20-9.62 (Fig. 10B). However, despite the large variation of the $^{87}Sr/^{86}Sr_i$ in the early phase basalts, their Nd-Hf isotope is relative homogenous and show no trends in the Sr-$\varepsilon_{Nd}(t)$ and $\varepsilon_{Nd}(t)$ - $\varepsilon_{Hf}(t)$ diagrams. In contrast, the late phase basalts have a relatively large range of $\varepsilon_{Nd}(t)$ (0.06-4.17) and $\varepsilon_{Hf}(t)$ (1.49-8.38) values, and their $^{87}Sr/^{86}Sr_i$ ratios range from 0.7041 to 0.7052. Note that there is a negative correlation between the Sr-Nd isotopic compositions of the late rift phase basalts (Fig. 10A), while the Nd-Hf isotopic compositions show a positive correlation (Fig. 10B).

5. Discussion

5.1 Evolution of multiphase rifting and volcanism

The temporal and spatial variations of the fault activity rates of the major faults in the Jianghan Basin are shown in Fig. 8, along with two stratal thickness profiles across the West Jianghan Basin and East Jianghan Basin. From the Shashi Stage (65-56 Ma) to the Xin'gouzui Stage (56-50 Ma), while fault activity decayed in the West Jianghan Basin, the fault activity rates of the major faults in the East Jianghan Basin generally increased (Fig. 8A, B). From the Jingsha Stage (50-45 Ma) to Jinghezhen Stage (32-26 Ma), although fault activity rates gradually decreased, the difference between the West Jianghan Basin and East Jianghan Basin increased (Fig.

8C, D and E), resulting in an eastward migration. This was due to the much rapider decrease of fault activity in the West Jianghan Basin than the East Jianghan Basin. Therefore, there is a progressively eastward migration of fault activity in the Jianghan Basin. Notably, the two-phase rifting displays two distinct intense-to-weak cycles in fault activity and fault activity rates during the late rift phase are significantly higher than the early rift phase (Fig. 8).

Sediment distribution is predominantly fault controlled and should be an accurate measure of the activity of major faults and basin subsidence with sufficient sedimentation rates (Nixon et al., 2016). The maximum sediment thickness of the Shashi Formation in the West Jianghan Basin is ca. 3400 m, significantly much thicker than that in the East Jianghan Basin (ca. 550 m) (Fig. 8A). The difference on sediment thickness of the Xin'gouzui Formation between the West Jianghan Basin and the East Jianghan Basin is significantly reduced, with the maximum unit thickness at ca. 1100 m in the West Jianghan Basin and ca. 950 m in the East Jianghan Basin (Fig. 8B). The maximum stratal thickness of the Jingsha Formation is ca. 2000 m in the West Jianghan Basin and ca. 3200 m in the East Jianghan Basin, which indicates that the maximum depocenter has shifted from the West Jianghan Basin to the East Jianghan Basin during the Jingsha Stage (Fig. 8C). During the Qianjiang-Jinghezhen Stage, depocentres continued migrating eastward, with the increasing difference on sediment thickness between the West Jianghan Basin and East Jianghan Basin (Fig. 8D, E). In summary, the same to the faulting, the depocentres of the Jianghan Basin also progressively migrated eastward (Fig. 8).

Volcanic activity was relatively weak and basaltic eruptions were scattered during the early rift phase (Fig. 8A, B). The area of the Xin'gouzui basalts was smaller than the Shashi basalts, showing a decayed trend of volcanic activity. The distribution of basalts during the late phase was almost contiguous. The basaltic eruption reached its peak during the Jingsha Stage (50-45 Ma) and then decreased moderately during the Qianjiang Stage (45-32 Ma). Clearly, the temporal variations of volcanic activity show two intense-to-weak cycles and significantly enhanced during the late rift phase, having a good correspondence with fault activity. In addition, there is no notable trend of the migration of volcanic activity, so the migration of volcanic activity is not taken into account when discussing the geodynamics of rifting and volcanism.

5.2 The origin of the Jianghan basalts

5.2.1 Post-magmatic alteration, crustal contamination and fractional crystallization

Low-pressure magmatic processes such as alteration, crustal contamination and fractional crystallization could significantly modify the composition of primary basaltic melt. Therefore, it is necessary to evaluate their potential effect before discussing source characteristics of the basalts.

Some samples with relatively high loss on ignition values (LOI; 2.11-6.34%), as well as a few secondary minerals (iddingsite and chlorite), indicates varying degrees of alteration. The effects of alteration on the incompatible trace elements can be examined via the correlations between fluid-mobile elements (e.g., Ba, Sr, Th, U, La, Nd) and fluid-immobile elements (e.g., Nb, Zr) (Fig. S5). The good correlations between Th, U, and Zr as well as La, Nd and Nb indicate that the effect of alteration is limited, while the early phase basalts have large variations of Sr values as well as $^{87}Sr/^{86}Sr_i$ ratios (Figs. 10A, S5E). This phenomenon can be well explained by the addition of seawater-altered oceanic crust in the source region (cf. Xu, 2014), as seawater is extremely low in Nd concentration (O’Nions et al., 1978) and seawater-altered oceanic basalt displays a relatively constant ε_{Nd} and a wide range of $^{87}Sr/^{86}Sr$ ratios (McCulloch et al., 1980). Thus we will not consider the $^{87}Sr/^{86}Sr_i$ in the following discussion.

Previous studies on the Cenozoic basalts from the eastern SCB suggested negligible crustal contamination (Li et al., 2015b, 2016b; Liu et al., 2016; Chu et al., 2017; Zeng et al., 2017). Trace element compositions of the Jianghan basalts also show no obvious imprint of continent crust in the spidergram (e.g., depletions in Nb and Ta; Rudnick and Gao, 2003) (Fig. 9b), with high $[Nb/Th]_N$ and $[Ta/U]_N$ ratios in all the basalts (Fig. 11a). As shown in Fig. 11b, most samples plot within the field of MORB and OIB (Nb/U = 47 ± 10; Hofmann et al., 1986) and their Nb/U ratios (30.0-52.7) are much higher than the continental crust (6.15; Rudnick and Gao, 2003). All these observations indicate that the Jianghan basalts suffered negligible crustal contamination.

The studied samples have evolved character with $Mg^{\#}$ ranging from 0.54 to 0.62 and low Ni (120-244 ppm) and Cr (181-416 ppm) contents (Fig. S4G, H), suggesting fractionation of olivine and clinopyroxene. The slightly negative correlation between SiO_2 and MgO (Fig. S4B) is also consistent with olivine and clinopyroxene fractionation, although Al_2O_3, $Fe_2O_3^T$ do not correlate with MgO (Fig. S4C, F). In addition, the absence of Eu anomalies (Fig. 9a) indicates plagioclase removal is minimal. However, the ratios of incompatible trace elements are not sensitive to fractional crystallization of olivine and clinopyroxene, and thus the observed geochemical features in these basalts reflect their source regions.

5.2.2 The asthenospheric mantle source character of the Jianghan basalts

The Cenozoic basalts in the eastern SCB are proposed to be derived from partial melting of the asthenosphere (Fig. 10A; Li et al., 2015b, 2016b). The enriched components have been attributed to the contributions from the stagnant Pacific slab (Li et al., 2015b, 2016b; Liu et al., 2016; Chu et al., 2017; Zeng et al., 2017; Sun et al., 2017). Regardless of some early phase basalts with high $^{87}Sr/^{86}Sr_i$ (see discussion in section 5.2), we propose that the Jianghan basalts were also derived from partial melting of asthenospheric mantle as all the samples plot in the MORB and OIB fields (Fig. 10). The Nb/U ratios of the Jianghan basalts are almost completely within the range of MORB + OIB (Nb/U = 47 ± 10; Hofmann et al., 1986) and Nb/La ratios (1.25-1.57) are higher than that in melts of lithospheric origin (Nb/La < 1; Smith et al., 1999), also suggesting their asthenospheric origin.

The early phase basalts have an almost homogeneous mantle source with limited $\varepsilon_{Nd}(t)$ and $\varepsilon_{Hf}(t)$ values, whereas the late phase basalts show a relatively large range of $\varepsilon_{Nd}(t)$ and $\varepsilon_{Hf}(t)$ values, indicating the compositional heterogeneity of the mantle source (Fig. 10). Furthermore, the source of the late phase basalts is isotopically slightly more enriched than the early phase basalts (Fig. 10).

5.2.3 Decreasing melting extent during progressive rifting

The late phase basalts have a higher abundances of incompatible elements (Fig. 9) and have greater $[La/Yb]_N$ ratios (5.50-10.29) than the early phase basalts ($[La/Yb]_N$ = 3.35-4.99). This may largely result from the smaller extent of partial melting of mantle source of the late phase basalts than the early phase basalts. The higher moderately/weakly incompatible element ratios of the late phase basalts also indicate a smaller extent of melting than the early phase basalts (Niu et al., 1996; Fig. 12). However, the classical rift development model argues that the lithosphere progressively thins as rifting proceeds (e.g., McKenzie, 1978; Fram and Lesher, 1993; Ziegler and Cloetingh, 2004; Rooney, 2010; Corti, 2012), which suggests a progressively thinner lithosphere in this area, and thus the extent of melting during the late rift phase should be greater than the early rift phase based on the “lid effect” (Ellam, 1992; Niu et al., 2011). Therefore, why do the late phase basalts have a smaller melting extent under a thinner lithosphere?

Niu (2005) proposed that decompression and volatile addition are two important processes in the production of basaltic magma in eastern China. Thus, the lithospheric thickness and the content of volatiles are two key constraints on the partial melting extent of asthenospheric mantle. Now that the late phase basalts have a smaller melting extent under a thinner lithosphere, we argue that the content of volatiles in the mantle source during the late rift phase was lower than the early rift phase, resulting in the mantle source having a higher solidus and smaller melting extent (cf. Gaetani and Grove, 1998; Niu, 2005; Niu et al., 2011, and references therein).

5.3 Geodynamic processes causing Cenozoic rifting and volcanism

5.3.1 Comparison of two alternative models

The Cenozoic geodynamics of the Jianghan Basin and eastern China remain controversial, as the involved rifting and volcanism are considered to have been driven either by Pacific plate motion or India-Asia collision (Fig. 2B and C). Therefore, the key to differentiating the two models is to distinguish whether the evolution of the Cenozoic rifting and volcanism in eastern China is coincident with Pacific plate motion or India-Asia collision processes. As a consequence, tectonic correlations between the Pacific plate motion, India-Asia collision, Jianghan Basin and eastern China are essential to settling the dispute (Fig. 13).

The rate of Pacific-Eurasia convergence varied significantly during the Cenozoic (Fig. 13; Engebretson, 1985; Northrup et al., 1995). The convergence rates began to decline at ca. 53 Ma and then increased at 40-37 Ma. If the extension of the lithosphere of eastern China was caused by the rollback of the subducted Pacific slab accompanied by the retreat of subduction zone, the low convergence rates may cause a much weaker extension of the lithosphere of eastern China, which were in conflict with a more intense rifting initiating in eastern China at the same time (e.g., Jianghan Basin, this study; Bohai Bay Basin, Ren et al., 2008). Furthermore, the passive rifting and upwelling model (Fig. 2B; e.g., Xu et al., 2012; Niu, 2013) cannot explain the widespread termination of rifting at ca. 26 Ma in eastern China in view of no significant change in Pacific plate motion at the same time (Fig. 13; Engebretson, 1985; Northrup et al., 1995). Importantly, there is no relevant response in eastern China to the sudden directional change of Pacific plate motion at ca. 50-47 Ma (Sharp and Clague, 2006; Torsvik et al., 2017). The increase of convergence rates at 40-37 Ma have a good accordance with some tectonic switches in eastern China, including the basaltic eruption gap in the eastern South China Block (38-17 Ma, Gong and Chen, 2014), depositional break and erosion in the Subei Basin (38-24 Ma, Qian, 2001; Liu et al., 2017), and dextral motion onset of the Tanlu Fault (ca. 40 Ma, Qi and Yang, 2010; Huang et al., 2015a). Therefore, it indicates that the motion of Pacific plate is considered to have caused compression and strike-slipping in eastern China during the Cenozoic, rather than extension.

The timing of the India-Asia collision onset is still hotly debated, and it is likely to have taken place anytime between ca. 65 Ma and ca. 50 Ma (e.g., Rowley, 1998; Yi et al., 2011; Meng et al., 2012; Van Hinsbergen et al., 2012; Zhu et al., 2015a; Hu et al., 2016; Ma et al., 2016). However, during the India-Asia collision processes, a series of significant changes in magmatic activity, sediment provenance, palaeomagnetic data and rate of convergence between India and Asia simultaneously occurred at ca. 50 Ma or slightly earlier (e.g., Patriat and Achache, 1984; Van Hinsbergen et al., 2011; Zhu et al., 2015a; Hu et al., 2016; Meng et al., 2017). The timing of these changes is coincident with the initiation of the late phase rifting in the Jianghan Basin. The primary phase of lithospheric removal beneath the Tibetan plateau occurred at ~26 Ma (Chung et al., 2005), corresponding with the widespread termination of rifting in eastern China (Fig. 13).

Therefore, the tectonic and magmatic phases in the Jianghan Basin and eastern China coincide with India-Asia collision events rather than Pacific plate motion.

In addition, it is also important to consider if the geochemical signatures have a greater affinity to one of the two models. As discussed above, the asthenospheric mantle source of the late phase basalts is isotopically slightly more enriched and heterogenous and has a smaller melting extent than the early phase basalts. An explanation for these observations can be made in the context of the passive rifting and upwelling model (Fig. 2B). As volatiles entered the melts, volatile content in mantle source could be diluted as rifting proceeded. Therefore, despite the progressive thinning of the lithosphere during the late rift phase, the mantle source had a smaller extent of partial melting. However, as rifting and volcanism during the early rift phase is significantly much weaker than the late rift phase (Fig. 8), the volatile consumption during the early rift phase may be rather low. Consequently, the volatile content in the mantle source should not change noticeably between early and late rift phases. Furthermore, this model cannot explain why the mantle source of the late rift phase became isotopically more enriched and heterogenous.

Numerous studies have proposed that the long-term (Triassic- Cretaceous) dehydration of the subducted Pacific slab played a key role in lithospheric thinning beneath eastern China (Niu, 2005; Windley et al., 2010; Li et al., 2012a, 2015a; Zhu et al., 2015b). Therefore, the asthenospheric mantle beneath thinner lithosphere (east of the NSGL) could be wet and abundant in volatiles (cf. Niu, 2005; Li et al., 2012a), while the asthenospheric mantle beneath thicker lithosphere (west of the NSGL) was nearly dry or with low volatile content. In the active rifting and upwelling model (Fig. 2C; Flower et al., 2001; Niu, 2005; Liu et al., 2004; Sun et al., 2017), the much more intense rifting and volcanism during the late rift phase implied a much larger scale of asthenospheric flow than the early rift phase. The more replenishment from west of the NSGL during the late rift phase could make the content of volatiles in the mixed mantle sources drop sharply as a result of dilution, resulting in the mixed mantle sources having a higher solidus and smaller melting extent (cf. Gaetani and Grove, 1998; Niu, 2005; Niu et al., 2011, and references therein). Lithospheric erosion occurred while asthenosphere flowed eastward, especially near the NSGL where asthenospheric flow experienced an intense upwelling, which has been verified by the Cenozoic lithospheric thinning to west of NSGL in the North China Block (e.g., Guo et al., 2014). While the much larger scale of asthenospheric flow passed through the NSGL, a much more intense lithospheric erosion occurred, capturing more ancient enriched material. The incorporation of more ancient enriched material into the upwelling asthenospheric mantle during the late rift phase could make the mantle source not only more enriched in Nd-Hf isotopes, but also compositionally heterogeneous (Fig. 10).

Other than the Cenozoic lithospheric thinning to west of NSGL (e.g., Guo et al., 2014), additional other observations support the active rifting and upwelling model. 1) As there is an inverse relationship between the extension in eastern China and the Pacific plate motion, the change of Pacific plate motion may be likely caused by the resistance of collision-induced eastward asthenospheric flow (cf. Flower et al., 2001). The main significance of the subducted Pacific plate during the Cenozoic maybe just contribute materials (such as volatiles, recycled oceanic crust, marine sediments and hydrous low-F melts) to the upper mantle beneath eastern China through dehydration in the MTZ (e.g., Xu et al., 2014; Li et al., 2016a, b; Liu et al., 2016; Guo et al., 2016; Chen et al., 2017), not the driving force for rifting and volcanism. 2) Asthenospheric flow has been detected by geophysical observations (seismic images) in the South

China Block (Huang et al., 2015b) and North China Block (Yu and Chen, 2016).

5.3.2 Preferred model and dynamic processes

The multidisciplinary evidence integrating our data and previous work provides an excellent opportunity for us to decipher the origin of the Cenozoic intracontinental rifting and volcanism in eastern China. Notably, the tectonic evolution of the Jianghan Basin and eastern China is coincident with India-Asia collision processes while it is mostly in conflict with Pacific plate motion based on the above discussion. Therefore, we prefer the active rifting and upwelling model in this study. Based on the temporal and spatial variations of rifting and volcanism unraveled by this study, we present an improved conceptual model (Fig. 14) to illustrate how eastward asthenospheric flow drove the development of the Jianghan Basin and caused relevant shallow responses.

During the Shashi Stage (65-56 Ma), with ongoing subduction of the India plate and the initial development of India-Asia collision (Fig. 13), asthenospheric mantle continued to be extruded laterally, leading to the development of asthenospheric mantle flowing eastward beneath eastern China (Fig. 14A). The eastward asthenospheric flow experienced a buoyant upwelling and decompression when flowing through the NSGL (Raddick et al., 2002; Niu, 2005). Under the diapirism of active upwelling mantle, the lithosphere beneath the Jianghan Basin was induced to magmatically rift. The reduction in fault and volcanic activity during the Xin'gouzui Stage (56-50 Ma) implies a reduction of flow at this time (Fig. 8), while the continuous eastward flow induced migration of rifting and depocentres towards the east (Fig. 14B). The intensity of India-Asia collision significantly increased at 50 Ma or slightly earlier (Fig. 13; e.g., Meng et al., 2012; Van Hinsbergen et al., 2011; Zhu et al., 2015a; Hu et al., 2016), resulting in a much enhanced asthenospheric mantle flow. The late phase of rifting in the Jianghan Basin initiated when this new wave of asthenospheric flow arrived (Fig. 14C). This greatly enhanced asthenospheric flow caused the lithosphere to be intensely extended, resulting in large scale of rifting and basaltic volcanism occurring in the Jianghan Basin. Meanwhile, rifting and depocentres continued to migrate eastward. During the Qianjiang Stage (45-32 Ma), the eastward asthenospheric flow reduced moderately as did the rifting and volcanism in the Jianghan Basin (Fig. 14D), while the eastward migration of rifting and depocentres continued. The eastward asthenospheric flow further decayed during the Jinghezhen Stage (32-26 Ma) (Fig. 14E), leading to rifting and volcanism greatly decaying. At ca. 26 Ma, the thickened lithosphere of the Tibetan Plateau was mostly removed (Chung et al., 2005) and the thick lithosphere to west of NSGL (stable craton with > 150 km thick lithosphere, Zhu et al., 2015b) is likely to have blocked the eastward asthenospheric flow (cf. Gong and Chen, 2014), resulting in the significant decrease of eastward asthenospheric flow beneath eastern China. This decayed asthenospheric flow cannot drive further extension of the lithosphere, so all the rift basins failed at ca. 26 Ma.

During the Cenozoic, the asthenospheric mantle to east of the NSGL was considered to be wet and abundant in volatiles (cf. Niu, 2005; Li et al., 2012a), while the asthenospheric mantle to west of the NSGL was nearly dry or with low volatile content. During the late rift phase, the much larger scale of volatile-poor asthenospheric flow during the late rift phase greatly diluted the mixed mantle sources and lowered the content of volatiles. As a result, although lithosphere got thinner during the late rift phase, the mixed mantle sources had a higher solidus than the early phase (e.g., Gaetani and Grove, 1998; Niu, 2005). Consequently, the late phase basalts show a lower extent of partial melting (Fig. 12). In addition, during the late rift phase, while the much larger late phase asthenospheric flow passed through the NSGL (Fig. 14C, D), the more intense lithospheric erosion made more ancient enriched material add into the mantle source, resulting in the mantle source becoming isotopically more enriched and heterogeneous (Fig. 10).

6. Conclusions

In this study, we investigate the temporal and spatial variations of rifting and volcanism in the Jianghan Basin. Both rifting and volcanism in the Jianghan Basin show two intense-to-weak cycles and significantly enhanced during the late rift phase. Meanwhile, rifting and depocentres progressively migrated eastward. Although all the Jianghan basalts share an asthenospheric origin, the source of the late phase basalts is isotopically slightly more enriched and heterogenous than that of the early phase basalts. The late phase basalts also display a smaller extent of partial melting even under a thinner lithosphere. By considering the evolution of the Jianghan Basin within a regional context, we propose that the passive rifting and upwelling model is incompatible with our observations and the tectonic evolution of the Jianghan Basin and eastern China has been at a first order controlled by Indian-Asia collision. The variations of rifting and volcanism in the Jianghan Basin indicate a multiphase and eastward asthenospheric flow beneath eastern China which experienced an intense upwelling when passing through the NSGL. The resulting model of the evolution of the Jianghan Basin, therefore, provides a unique insight into the development of an intracontinental rift and volcanic province and suggests that asthenospheric flow plays a much more important role in the regions where there are step changes in lithospheric thickness than previously considered.

Acknowledgments

We thank Patrick W. Ball and an anonymous reviewer for their constructive comments and suggestions which have significantly improved our manuscript. Associate Editor Nicholas Rawlinson is thanked for his helpful comments and editorial handling. We are grateful to Rong Xu, Hongyan Li, Xiangdong Wang, Jian Ma and Yanqing Li for early discussion and data analysis. We also thank Prof. Lian Zhou, Lanping Feng, Yating Hu and Haihong Chen for bulk-rock Sr-Nd isotope and trace element measurements as well as Jianpei Lu and Manrong Jiang for petrography analysis. This work was financially supported by the Natural Science Foundation of Hubei Province (2016CFA084), the Major National Science and Technology Programs, China (2016ZX05002-006), the Scientific Research Project of China Petroleum and Chemical Corporation (P14111) and the National Natural Science Foundation of China (NSFC grant 41776067).

Appendix A. Supplementary material

This excel file includes detailed sample locations, whole-rock geochemical data and thickness data of basalts of different stages in basalt-encountered wells.

Appendix B. Supplementary material

This file includes detailed analytical methods of whole-rock major, trace elements and Sr-Nd-Hf isotopes and supplementary figures S1-S5.

References

Allègre, C.J., 1982. Chemical geodynamics. Tectonophysics 81(3), 109-132. DOI: https://doi.org/10.1016/0040-1951(82)90125-1.

Besse, J., Courtillot, V., Pozzi, J.P., Westphal, M., Zhou, Y.X., 1984. Palaeomagnetic estimates of crustal shortening in the Himalayan thrusts and Zangbo suture. Nature 311, 621-626. DOI: 10.1038/311621a0.

Bryan, S.E., Ferrari, L., 2013. Large igneous provinces and silicic large igneous provinces: Progress in our understanding over the last 25 years. Geological Society of America Bulletin 125(7-8), 1053-1078. DOI: 10.1130/B30820.1.

Chen, H., Xia, Q., Ingrin, J., Deloule, E., Bi, Y., 2017. Heterogeneous source components of intraplate basalts from NE China induced by the ongoing Pacific slab subduction. Earth and Planetary Science Letters 459, 208-220. DOI: 10.1016/j.epsl.2016.11.030.

Childs, C., Nicol, A., Walsh, J.J., Watterson, J., 2003. The growth and propagation of synsedimentary faults. Journal of Structural Geology 25(4), 633-648. DOI: https://doi.org/10.1016/S0191-8141(02)00054-8.

Chu, Z., Yan, Y., Zeng, G., Tian, W., Li, C., Yang, Y., Guo, J., 2017. Petrogenesis of Cenozoic basalts in central-eastern China: Constraints from Re–Os and PGE geochemistry. Lithos 278-281, 72-83. DOI: 10.1016/j.lithos.2017.01.022.

Chung, S., Chu, M., Zhang, Y., Xie, Y., Lo, C., Lee, T., Lan, C., Li, X., Zhang, Q., Wang, Y., 2005. Tibetan tectonic evolution inferred from spatial and temporal variations in post-collisional magmatism. Earth-Science Reviews 68(3-4), 173-196. DOI: 10.1016/j.earscirev.2004.05.001.

Chung, S., Lo, C., Lee, T., Zhang, Y., Xie. Y., Li, X., Wang, K., Wang, P., 1998. Diachronous uplift of the Tibetan plateau starting 40 Myr ago. Nature 394, 769-773. DOI: 10.1038/29511.

Conrad, C.P., Bianco, T.A., Smith, E.I., Wessel, P., 2011. Patterns of intraplate volcanism controlled by asthenospheric shear. Nature Geoscience 4(5), 317-321. DOI: 10.1038/ngeo1111.

Corti, G., 2012. Evolution and characteristics of continental rifting: Analog modeling-inspired view and comparison with examples from the East African Rift System. Tectonophysics 522-523, 1-33. DOI: 10.1016/j.tecto.2011.06.010.

Corti, G., Bonini, M., Conticelli, S., Innocenti, F., Manetti, P., Sokoutis, D., 2003. Analogue modelling of continental extension: a review focused on the relations between the patterns of deformation and the presence of magma. Earth-Science Reviews 63(3-4), 169-247. DOI: 10.1016/S0012-8252(03)00035-7.

Davies, D.R., Rawlinson, N., 2014. On the origin of recent intraplate volcanism in Australia. Geology 42(12), 1031-1034. DOI: https://doi.org/10.1130/G36093.1.

Engebretson, D.C., Cox, A., Gordon, R.G., 1985. Relative Motions Between Oceanic and Continental Plates in the Pacific Basin: Geological Society of America Special Paper 206, 1-59. DOI: https://doi.org/10.1130/SPE206-p1.

Ellam, R.M., 1992. Lithospheric thickness as a control on basalt geochemistry. Geology 20(2), 153. DOI: 10.1130/0091-7613(1992)020<0153:LTAACO>2.3.CO;2.

Flower, M.F.J., Russo, R.M., Tamaki, K., Hoang, N., 2001. Mantle contamination and the Izu-Bonin-Mariana (IBM) ‘high-tide mark’: evidence for mantle extrusion caused by Tethyan closure. Tectonophysics 333(1-2), 9-34. DOI: https://doi.org/10.1016/S0040-1951(00)00264-X.

Fram, M.S., Lesher, C.E., 1993. Geochemical constraints on mantle melting during creation of the North Atlantic basin. Geology 363(6431), 712-715. DOI: 10.1038/363712a0.

Gaetani, G.A., Grove, T.L., 1998. The influence of water on melting of mantle peridotite. Contributions to Mineralogy and Petrology 131(4), 323-346. DOI: 10.1007/s004100050396.

Gong, J., Chen, Y.J., 2014. Evidence of lateral asthenosphere flow beneath the South China craton driven by both Pacific plate subduction and the India-Eurasia continental collision. Terra Nova 26(1), 55-63. DOI: 10.1111/ter.12069.

Guo, P., Niu, Y., Sun, P., Ye, L., Liu, J., Zhang, Y., Feng, Y., Zhao, J., 2016. The origin of Cenozoic basalts from central Inner Mongolia, East China: The consequence of recent mantle metasomatism genetically associated with seismically observed paleo-Pacific slab in the mantle transition zone. Lithos 240-243, 104-118. DOI: 10.1016/j.lithos.2015.11.010.

Guo, P., Niu, Y., Ye, L., Liu, J., Sun, P., Cui, H., Zhang, Y., Gao, J., Su, L., Zhao, J., Feng, Y., 2014. Lithosphere thinning beneath west North China Craton: Evidence from geochemical and Sr–Nd–Hf isotope compositions of Jining basalts. Lithos 202-203, 37-54. DOI: 10.1016/j.lithos.2014.04.024.

Harangi, S., Jankovics, M.É., Sági, T., Kiss, B., Lukács, R., Soós, I., 2015. Origin and geodynamic relationships of the Late Miocene to Quaternary alkaline basalt volcanism in the Pannonian basin, eastern–central Europe. International Journal of Earth Sciences 104(8), 2007-2032. DOI: 10.1007/s00531-014-1105-7.

HBGMR (Hubei Bureau of Geology and Mineral Resources), 1990. Regional Geology of the Hubei Province. Geological Press, Beijing (in Chinese with English summary).

Hofmann, A.W., Jochum, K.P., Seufert, M., White, W.M., 1986. Nb and Pb in oceanic basalts:

new constraints on mantle evolution. Earth and Planetary Science Letters 79(1), 33-45. DOI: 10.1016/0012-821X(86)90038-5.

Hu, X., Garzanti, E., Wang, J., Huang, W., An, W., Webb, A., 2016. The timing of India-Asia collision onset – Facts, theories, controversies. Earth-Science Reviews 160, 264-299. DOI: 10.1016/j.earscirev.2016.07.014.

Huang, J., Zhao, D., 2006. High-resolution mantle tomography of China and surrounding regions. Journal of Geophysical Research 111(B9). DOI: 10.1029/2005JB004066.

Huang, L., Liu, C., 2014. Evolutionary characteristics of the sags to the east of Tan–Lu Fault Zone, Bohai Bay Basin (China): Implications for hydrocarbon exploration and regional tectonic evolution. Journal of Asian Earth Sciences 79, 275-287. DOI: https://doi.org/10.1016/j.jseaes.2013.09.031.

Huang, L., Liu, C., Kusky, T.M., 2015a. Cenozoic evolution of the Tan–Lu Fault Zone (East China)—Constraints from seismic data. Gondwana Research 28(3), 1079-1095. DOI: 10.1016/j.gr.2014.09.005.

Huang, Z., Wang, P., Xu, M., Wang, L., Ding, Z., Wu, Y., Xu, M., Mi, N., Yu, D., Li, H., 2015b. Mantle structure and dynamics beneath SE Tibet revealed by new seismic images. Earth and Planetary Science Letters 411, 100-111. DOI: http://dx.doi.org/10.1016/j.epsl.2014.11.040.

Ivanov, A.V., Demonterova, E.I., He, H., Perepelov, A.B., Travin, A.V., Lebedev, V.A., 2015. Volcanism in the Baikal rift: 40years of active-versus-passive model discussion. Earth-Science Reviews 148, 18-43. DOI: 10.1016/j.earscirev.2015.05.011.

Jackson, C.A.L., 2012. Seismic reflection imaging and controls on the preservation of ancient sill-fed magmatic vents. Journal of the Geological Society 169(5), 503-506. DOI:

10.1144/0016-76492011-147.

Jiang, M., Ai, Y., Chen, L., Yang, Y., 2013. Local modification of the Lithosphere beneath the central and western North China Craton: 3-D constraints from Rayleigh wave tomography. Gondwana Research 24, 849-864. DOI: http://dx.doi.org/10.1016/j.gr.2012.06.018.

Kuritani, T., Kimura, J., Ohtani, E., Miyamoto, H., Furuyama, K., 2013. Transition zone origin of potassic basalts from Wudalianchi volcano, northeast China. Lithos 156-159, 1-12. DOI: 10.1016/j.lithos.2012.10.010.

Le Bas, M.J., Le Maitre, R.W., Strekeisen, A., Zanettin, B., 1986. A Chemical classification of volcanic rocks based on the total alkali-silica diagram. Journal of Petrology 27, 745–750. DOI: https://doi.org/10.1093/petrology/27.3.745.

Lebedev, S., Meier, T., van der Hilst, R.D., 2006. Asthenospheric flow and origin of volcanism in the Baikal Rift area. Earth and Planetary Science Letters 249(3-4), 415-424. DOI: 10.1016/j.epsl.2006.07.007.

Li, H., Xu, Y., Ryan, J.G., Huang, X., Ren, Z., Guo, H., Ning, Z., 2016a. Olivine and melt inclusion chemical constraints on the source of intracontinental basalts from the eastern North China Craton: Discrimination of contributions from the subducted Pacific slab. Geochimica et Cosmochimica Acta 178, 1-19. DOI: 10.1016/j.gca.2015.12.032.

Li, J., Bi, S., Selby, D., Chen, L., Vasconcelos, P., Thiede, D., Zhou, M., Zhao, X., Li, Z., Qiu, H., 2012a. Giant Mesozoic gold provinces related to the destruction of the North China craton. Earth and Planetary Science Letters 349-350, 26-37. DOI: 10.1016/j.epsl.2012.06.058.

Li, J., Zhang, Y., Dong, S., Johnston, S.T., 2014. Cretaceous tectonic evolution of South China: A preliminary synthesis. Earth-Science Reviews 134, 98-136. DOI:

10.1016/j.earscirev.2014.03.008.

Li, S., Suo, Y., Dai, L., Liu, L., Jin, C., Liu, X., Hao, T., Zhou, L., Liu, B., Zhou, J., Jiao, Q., 2010. Development of the Bohai Bay Basin and destruction of the North China Craton. Earth Science Frontiers 17(4), 64-89 (in Chinese with English abstract).

Li, S., Suo, Y., Santosh, M., Dai, L., Liu, X., Yu, S., Zhao, S., Jin, C., 2013. Mesozoic to Cenozoic intracontinental deformation and dynamics of the North China Craton. Geological Journal 48, 543-560. DOI: 10.1002/gj.2500.

Li, X., Zhu, P., Kusky, T.M., Gu, Y., Peng, S., Yuan, Y., Fu, J., 2015a. Has the Yangtze craton lost its root? A comparison between the North China and Yangtze cratons. Tectonophysics 655, 1-14. DOI: 10.1016/j.tecto.2015.04.008.

Li, Y., Ma, C., Robinson, P.T., 2016b. Petrology and geochemistry of Cenozoic intra-plate basalts in east-central China: Constraints on recycling of an oceanic slab in the source region. Lithos 262, 27-43. DOI: 10.1016/j.lithos.2016.06.012.

Li, Y., Ma, C., Robinson, P.T., Zhou, Q., Liu, M., 2015b. Recycling of oceanic crust from a stagnant slab in the mantle transition zone: Evidence from Cenozoic continental basalts in Zhejiang Province, SE China. Lithos 230, 146-165. DOI: 10.1016/j.lithos.2015.05.021.

Li, Z., Li, X., Chung, S., Lo, C., Xu, X., Li, W., 2012b. Magmatic switch-on and switch-off along the South China continental margin since the Permian: Transition from an Andean-type to a Western Pacific-type plate boundary. Tectonophysics 532-535, 271-290. DOI: 10.1016/j.tecto.2012.02.011.

Liu, M., Cui, X., Liu, F., 2004. Cenozoic rifting and volcanism in eastern China: a mantle dynamic link to the Indo–Asian collision? Tectonophysics 393(1-4), 29-42. DOI:

10.1016/j.tecto.2004.07.029.

Liu, S., Xia, Q., Choi, S.H., Deloule, E., Li, P., Liu, J., 2016. Continuous supply of recycled Pacific oceanic materials in the source of Cenozoic basalts in SE China: the Zhejiang case. Contributions to Mineralogy and Petrology 171(12). DOI: 10.1007/s00410-016-1310-4.

Liu, Y., Chen, Q., Wang, X., Hu, K., Cao, S., Wu, L., Gao, F., 2017. Influence of normal fault growth and linkage on the evolution of a rift basin: A case from the Gaoyou depression of the Subei Basin, eastern China. AAPG Bulletin 101(02), 265-288. DOI: 10.1306/06281615008.

Ma, Y., Yang, T., Bian, W., Jin, J., Zhang, S., Wu, H., Li, H., 2016. Early Cretaceous paleomagnetic and geochronologic results from the Tethyan Himalaya: Insights into the Neotethyan paleogeography and the India–Asia collision. Scientific Reports 6(1). DOI: 10.1038/srep21605.

McCulloch, M.T., Gregory, R.T., Wasserburg, G.J., Taylor, H.P., 1980. A neodymium, strontium, and oxygen isotopic study of the Cretaceous Samail ophiolite and implications for the petrogenesis and seawater-hydrothermal alteration of oceanic crust. Earth and Planetary Science Letters 46(2), 201-211. DOI: https://doi.org/10.1016/0012-821X(80)90006-0.

McKenzie, D., 1978. Some remarks on the development of sedimentary basins. Earth and Planetary Science Letters 40, 25-32.

Meng, J., Coe, R.S., Wang, C., Gilder, S.A., Zhao, X., Liu, H., Li, Y., Ma, P., Shi, K., Li, S., 2017. Reduced convergence within the Tibetan Plateau by 26 Ma? Geophysical Research Letters 44(13), 6624-6632. DOI: 10.1002/2017GL074219.

Meng, J., Wang, C., Zhao, X., Coe, R., Li, Y., Finn, D., 2012. India-Asia collision was at 24°N and 50 Ma: palaeomagnetic proof from southernmost Asia. Scientific Reports 2(1). DOI:

10.1038/srep00925.

Niu, Y., 2005. Generation and Evolution of Basaltic Magmas: Some Basic Concepts and a New View on the Origin of Mesozoic- Cenozoic Basaltic Volcanism in Eastern China. Geological journal of China universities 11, 9-46.

Niu, Y., 2013. Subduction initiation, trench retreat and global tectonic consequences: The origin of backarc basins in the western Pacific and effect on eastern China geology since the Mesozoic. In Zhai, G., Xiao, W. Plate Tectonics, Geological Events and Resources: New Advances in Geological Sciences. Science Press, Beijing, P. 1-25 (in Chinses).

Niu, Y., Batiza, R., 1997. Trace element evidence from seamounts for recycled oceanic crust in the Eastern Pacific mantle. Earth and Planetary Science Letters 148(3–4), 471-483. DOI: https://doi.org/10.1016/S0012-821X(97)00048-4.

Niu, Y., Regelous, M., Wendt, I.J., Batiza, R., O Hara, M.J., 2002. Geochemistry of near-EPR seamounts: importance of source vs. process and the origin of enriched mantle component. Earth and Planetary Science Letters 199(3–4), 327-345. DOI: https://doi.org/10.1016/S0012-821X(02)00591-5.

Niu, Y., Waggoner, D. G., Sinton, J. M., Mahoney, J. J., 1996. Mantle source heterogeneity and melting processes beneath seafloor spreading centers: The East Pacific Rise, 18°–19°S. Journal of Geophysical Research 101(B12), 27711–27733. DOI: 10.1029/96JB01923.

Niu, Y., Wilson, M., Humphreys, E.R., O'Hara, M.J., 2011. The Origin of Intra-plate Ocean Island Basalts (OIB): the Lid Effect and its Geodynamic Implications. Journal of Petrology 52(7-8), 1443-1468. DOI: 10.1093/petrology/egr030.

Nixon, C.W., McNeill, L.C., Bull, J.M., Bell, R.E., Gawthorpe, R.L., Henstock, T.J., Christodoulou, D., Ford, M., Taylor, B., Sakellariou, D., Ferentinos, G., Papatheodorou, G., Leeder, M.R., Collier, R.E.L., Goodliffe, A.M., Sachpazi, M., Kranis, H., 2016. Rapid spatiotemporal variations in rift structure during development of the Corinth Rift, central Greece. Tectonics 35(5), 1225-1248. DOI: 10.1002/2015TC004026.

Northrup, C.J., Royden, L.H., Burchfiel, B.C., 1995. Motion of the Pacific plate relative to Eurasia and its potential relation to Cenozoic extension along the eastern margin of Eurasia. Geology 23(8), 719-722. DOI: org/10.1130/0091-7613(1995)023<0719:MOTPPR>2.3.CO;2.

Noury, M., Philippon, M., Bernet, M., Paquette, J., Sempere, T., 2017. Geological record of flat slab–induced extension in the southern Peruvian forearc. Geology, G38990.1. DOI: 10.1130/G38990.1.

O'Nions, R.K., Carter, S.R., Cohen, R.S., Evensen, N.M., Hamilton, P.J., 1978. Pb, Nd and Sr isotopes in oceanic ferromanganese deposits and ocean floor basalts. Nature 273, 435-438.

Patriat, P. and Achache, J, 1984. India-Eurasia collision chronology has implications for crustal shortening and driving mechanism of plates. Nature 311, 615–621. DOI: 10.1038/311615a0.

Peng T., Wang, Y., Fan, W., Yu, X., Peng, B., Xu, Z., 2006. ^{39}Ar/^{40}Ar geochronology and Geochemistry of the early Tertiary basaltic rocks in the Jianghan Basin, China and its petrogenesis. Acta Petrologica Sinica 22(6), 1617-1626 (in Chinese with English abstract).

Petit, C., Déverchère, J., 2006. Structure and evolution of the Baikal rift: A synthesis. Geochemistry, Geophysics, Geosystems 7(11), n/a-n/a. DOI: 10.1029/2006GC001265.

Porter, R.C., Fouch, M.J., Schmerr, N.C., 2014. Dynamic lithosphere within the Great Basin. Geochemistry, Geophysics, Geosystems 15(4), 1128-1146. DOI: 10.1002/2013GC005151.

Putirka, K., Platt, B., 2012. Basin and Range volcanism as a passive response to extensional tectonics. Geosphere 8(6), 1274-1285. DOI: 10.1130/GES00803.1.

Qi, J., Yang, Q., 2010. Cenozoic structural deformation and dynamic processes of the Bohai Bay basin province, China. Marine and Petroleum Geology 27(4), 757-771. DOI: 10.1016/j.marpetgeo.2009.08.012.

Qian, J., 2001. Oil and gas fields formation and distribution of Subei Basin-Research compared to Bohai Bay Basin. Acta Petrolei Sinica 22(3), 12-16 (in Chinese with English abstract).

Raddick, M.J., Parmentier, E.M., Scheirer, D.S., 2002. Buoyant decompression melting: A possible mechanism for intraplate volcanism. Journal of Geophysical Research: Solid Earth 107(B10), ECV 7-1-ECV 7-14. DOI: 10.1029/2001JB000617.

Ren, F., Liu, Z., Qiu, L., Han, L., Zhou, L., 2008. Space-time discrepancy of depressional evolution in the Bohai Bay Basin during the Cenozoic. Chinese Journal of Geology 43(3), 546-557 (in Chinese with English abstract).

Ren, J., Tamaki, K., Li, S., Junxia, Z., 2002. Late Mesozoic and Cenozoic rifting and its dynamic setting in Eastern China and adjacent areas. 344(3), 175 - 205. DOI: 10.1016/S0040-1951(01)00271-2.

Rooney, T.O., 2010. Geochemical evidence of lithospheric thinning in the southern Main Ethiopian Rift. Lithos 117(1-4), 33-48. DOI: 10.1016/j.lithos.2010.02.002.

Rowley, D.B., 1998. Minimum Age of Initiation of Collision Between India and Asia North of Everest Based on the Subsidence History of the Zhepure Mountain Section. The Journal of Geology 106(2), 220-235. DOI: 10.1086/516018.

Rudnick, R.L., Gao, S., 2003. Composition of the continental crust. Treatise on Geochemistry 3, 1–64.

Sakuyama, T., Tian, W., Kimura, J., Fukao, Y., Hirahara, Y., Takahashi, T., Senda, R., Chang, Q., Miyazaki, T., Obayashi, M., Kawabata, H., Tatsumi, Y., 2013. Melting of dehydrated oceanic crust from the stagnant slab and of the hydrated mantle transition zone: Constraints from Cenozoic alkaline basalts in eastern China. Chemical Geology 359, 32-48. DOI: 10.1016/j.chemgeo.2013.09.012.

Sharp, W.D., Clague, D.A., 2006. 50-Ma Initiation of Hawaiian-Emperor Bend Records Major Change in Pacific Plate Motion. Science 313(5791), 1281. DOI: 10.1126/science.1128489.

Smith, E.I., Sánchez, A., Walker, J.D., Wang, K., 1999. Geochemistry of Mafic Magmas in the Hurricane Volcanic Field, Utah: Implications for Small‐ and Large‐Scale Chemical Variability of the Lithospheric Mantle. The Journal of Geology 107(4), 433-448. DOI: 10.1086/314355.

Stracke, A., Bizimis, M., Salters, V.J.M., 2003. Recycling oceanic crust: Quantitative constraints. Geochemistry, Geophysics, Geosystems 4(3). DOI: 10.1029/2001GC000223.

Stracke, A., Hofmann, A.W., Hart, S.R., 2005. FOZO, HIMU, and the rest of the mantle zoo. Geochemistry, Geophysics, Geosystems 6(5), n/a-n/a. DOI: 10.1029/2004GC000824.

Sun, P., Niu, Y., Guo, P., Ye, L., Liu, J., Feng, Y., 2017. Elemental and Sr–Nd–Pb isotope geochemistry of the Cenozoic basalts in Southeast China: Insights into their mantle sources and melting processes. Lithos 272-273, 16-30. DOI: 10.1016/j.lithos.2016.12.005.

Sun, S.S., McDonough, W.F., 1989. Chemical and isotopic systematics of oceanic basalts: implications for mantle composition and processes. Geological Society, London, Special Publications 42(1), 313. DOI: 10.1144/GSL.SP.1989.042.01.19.

Suo, Y., Li, S., Dai, L., Liu, X., Zhou, L., 2012. Cenozoic tectonic migration and basin evolution in East Asia and its continental margins. Acta Petrologica Sinica 28(8), 2602-2618 (in Chinese with English abstract).

Suo, Y., Li, S., Yu, S., Somerville, I.D., Liu, X., Zhao, S., Dai, L., 2014. Cenozoic tectonic jumping and implications for hydrocarbon accumulation in basins in the East Asia Continental Margin. Journal of Asian Earth Sciences 88, 28-40. DOI: 10.1016/j.jseaes.2014.02.019.

Tang, Y., Zhang, H., Ying, J., 2006. Asthenosphere–lithospheric mantle interaction in an extensional regime: Implication from the geochemistry of Cenozoic basalts from Taihang Mountains, North China Craton. Chemical Geology 233(3-4), 309-327. DOI: 10.1016/j.chemgeo.2006.03.013.

Taylor, S.K., Nicol, A., Walsh, J.J., 2008. Displacement loss on growth faults due to sediment compaction. Journal of Structural Geology 30(3), 394-405. DOI: 10.1016/j.jsg.2007.11.006.

Teng, C., Hao, F., Zou, H., Zhou, X., Xu, C., 2016. Tan-Lu fault system and its significance in oil accumulation in the central Liaodong Bay subbasin, Bohai Bay Basin, China. AAPG Bulletin 100(2), 289-314. DOI: 10.1306/10221515011.

Torsvik, T.H., Doubrovine, P.V., Steinberger, B., Gaina, C., Spakman, W., Domeier, M., 2017. Pacific plate motion change caused the Hawaiian-Emperor Bend. Nature Communications 8, 15660. DOI: 10.1038/ncomms15660.

Van Hinsbergen, D.J.J., Lippert, P.C., Dupont-Nivet, G., McQuarrie, N., Doubrovine, P.V., Spakman, W., Torsvik, T.H., 2012. Greater India Basin hypothesis and a two-stage Cenozoic collision between India and Asia. Proceedings of the National Academy of Sciences of the United States of America 109(20), 7659-7664. DOI: 10.1073/pnas.1117262109.

Van Hinsbergen, D.J.J., Steinberger, B., Doubrovine, P.V., Gassmöller, R., 2011. Acceleration and deceleration of India-Asia convergence since the Cretaceous: Roles of mantle plumes and continental collision. Journal of Geophysical Research 116(B6). DOI: 10.1029/2010JB008051.

Vervoort, J.D., Blichert-Toft, J., 1999. Evolution of the depleted mantle: Hf isotope evidence from juvenile rocks through time. Geochimica et Cosmochimica Acta 63(3), 533-556. DOI: https://doi.org/10.1016/S0016-7037(98)00274-9.

Wang, B., Lin, C., Chen, Y., Lu, M., Liu, J., 2006. Episodic tectonic movement and evolutional character in the Jianghan Basin. Oil Geophysical Prospecting 41(2), 226-230 (in Chinese with English abstract).

Wang, X., Wilde, S.A., Li, Q., Yang, Y., 2015. Continental flood basalts derived from the hydrous mantle transition zone. Nature Communications 6, 7700. DOI: 10.1038/ncomms8700.

Watson, D., Schofield, N., Jolley, D., Archer, S., Finlay, A.J., Mark, N., Hardman, J., Watton, T., 2017. Stratigraphic overview of Palaeogene tuffs in the Faroe − Shetland Basin, NE Atlantic Margin. Journal of the Geological Society 174(4), 627-645. DOI: 10.1144/jgs2016-132.

Wen, X., 2014. Tectonic features of the basins at the north margin of the South China Sea from Cretaceous to oldest Eogene. Master's Thesis, China University of Geosciences (Beijing) (in Chinese with English abstract).

Windley, B.F., Maruyama, S., Xiao, W.J., 2011. Delamination/thinning of sub-continental lithospheric mantle under Eastern China: The role of water and multiple subduction. American Journal of Science 310(10), 1250-1293. DOI: 10.2475/10.2010.03.

Wu, F., Xu, Y., Gao, S., Zheng, J., 2008. Lithospheric thinning and destruction of the North China

Craton. Acta Petrologica Sinica 24(6): 1145-1174 (in Chinese with English abstract).

Wu, L., Mei, L., Liu, Y., Paton, D.A., Luo, J., Yu, L., Wang, D., Min, C., Li, M., Guo, L., Wen, H, 2018. The stratigraphic and structural record of the Cretaceous Jianghan Basin, central China: Implications for initial rifting processes and geodynamics. Cretaceous Research 90, 21-39. DOI: https://doi.org/10.1016/j.cretres.2018.03.028.

Xu, L., Yan, C., Yu, H., Wang, B., 1995. Chronology of Paleogene volcanic rocks in the Jianghan Basin. Oil & Gas Geology 16(2), 132-137 (in Chinese with English abstract).

Xu, Y., 2007. Diachronous lithospheric thinning of the North China Craton and formation of the Daxin'anling–Taihangshan gravity lineament. Lithos 96(1-2), 281-298. DOI: 10.1016/j.lithos.2006.09.013.

Xu, Y., 2014. Recycled oceanic crust in the source of 90–40Ma basalts in North and Northeast China: Evidence, provenance and significance. Geochimica et Cosmochimica Acta 143, 49-67. DOI: 10.1016/j.gca.2014.04.045.

Xu, Y., Zhang, H., Qiu, H., Ge, W., Wu, F., 2012. Oceanic crust components in continental basalts from Shuangliao, Northeast China: Derived from the mantle transition zone? Chemical Geology 328, 168-184. DOI: 10.1016/j.chemgeo.2012.01.027.

Yi, Z., Huang, B., Chen, J., Chen, L., Wang, H., 2011. Paleomagnetism of early Paleogene marine sediments in southern Tibet, China: Implications to onset of the India–Asia collision and size of Greater India. Earth and Planetary Science Letters. DOI: 10.1016/j.epsl.2011.07.001.

Yin, A., 2010. Cenozoic tectonic evolution of Asia: A preliminary synthesis. Tectonophysics 488(1-4), 293-325. DOI: 10.1016/j.tecto.2009.06.002.

Yu, Y., Chen, Y.J., 2016. Seismic anisotropy beneath the southern Ordos block and the

Qinling-Dabie orogen, China: Eastward Tibetan asthenospheric flow around the southern Ordos. Earth and Planetary Science Letters 455, 1-6. DOI: 10.1016/j.epsl.2016.08.026.

Zeng, G., Chen, L., Yu, X., Liu, J., Xu, X., Erdmann, S., 2017. Magma-magma interaction in the mantle beneath eastern China. Journal of Geophysical Research: Solid Earth 122(4), 2763-2779. DOI: 10.1002/2017JB014023.

Zhao, D., Yu, S., Ohtani, E., 2011. East Asia: Seismotectonics, magmatism and mantle dynamics. Journal of Asian Earth Sciences 40(3), 689-709. DOI: 10.1016/j.jseaes.2010.11.013.

Zhao, F., Jiang, S., Li, S., Zhang, H., Wang, G., Lei, J., Gao, S., 2016. Cenozoic tectonic migration in the Bohai Bay Basin, East China. Geological Journal 51, 188-202. DOI: 10.1002/gj.2787.

Zhao, G., Wilde, S.A., Cawood, P.A., Sun, M., 2001. Archean blocks and their boundaries in the North China Craton: lithological, geochemical, structural and P–T path constraints and tectonic evolution. Precambrian Research 107(1), 45-73. DOI: https://doi.org/10.1016/S0301-9268(00)00154-6.

Zhu, D., Wang, Q., Zhao, Z., Chung, S., Cawood, P.A., Niu, Y., Liu, S., Wu, F., Mo, X., 2015a. Magmatic record of India-Asia collision. Scientific Reports 5(1), 14289. DOI: 10.1038/srep14289.

Zhu, G., Jiang, D., Zhang, B., Chen, Y., 2012. Destruction of the eastern North China Craton in a backarc setting: Evidence from crustal deformation kinematics. Gondwana Research 22(1), 86-103. DOI: 10.1016/j.gr.2011.08.005.

Zhu, R., Fan, H., Li, J., Meng, Q., Li, S., Zeng, Q., 2015b. Decratonic gold deposits. Science China Earth Sciences 58(9), 1523-1537. DOI: 10.1007/s11430-015-5139-x.

Ziegler, P.A., Cloetingh, S., 2004. Dynamic processes controlling evolution of rifted basins. Earth-Science Reviews 64(1-2), 1-50. DOI: 10.1016/S0012-8252(03)00041-2.

Zindler, A., Hart, S., 1986. Chemical Geodynamics. Annual Review of Earth and Planetary Sciences 14(1), 493-571. DOI: 10.1146/annurev.ea.14.050186.002425.

Figure captions

Fig. 1 Topographic map of China and neighboring regions (modified after Jiang et al., 2013). QDOB, Qinling-Dabie Orogenic Belt; NSGL, North–South Gravity Lineament; JHB, Jianghan Basin. The dashed lines (suture zones) mark the primary tectonic boundaries (after Zhao et al., 2001).

Fig. 2 (A) Simplified tectonic map showing the distribution of the Cenozoic rift basins (cf. Suo et al., 2012; Zhu et al., 2012; Wen, 2014) and basalts (Modified from Xu, 2007; Guo et al., 2016; Sun et al., 2017) in eastern China. Basin names: BBB, Bohai Bay Basin; WSB, West Sub-basin; CSB, Central Sub-basin; ESB, East Sub-basin; LB, Laiwu Basin; MB, Mengyin Basin; QB, Quanpu Basin; PB, Pingyi Basin; NB, Nanhuabei Basin; NXB, Nanxiang Basin; JHB, Jianghan Basin; SBB, Subei Basin; DB, Dongting Basin; PB, Poyanghu Basin; HB, Hengyang Basin; SSB, Sanshui Basin. See Fig. 1 for location. The eastward migration of faulting and depocentres of the Bohai Bay Basin is from Qi and Yang (2010), Suo et al. (2012, 2014) and Zhao et al. (2016). The eastward migration of volcanic activity in the eastern South China Block is from Gong and Chen (2014). Group A is basalts with ages older than 38 Ma; Group B is basalts with ages of 17-8 Ma;

Group C is basalts with ages younger than 8 Ma. (B-C) Competing models illustrating the distinct geodynamic origin for Cenozoic rifting and volcanism in eastern China: (B) Passive rifting and upwelling model (modified from Xu et al., 2012; Niu, 2013); (C) Active rifting and upwelling model (modified from Niu, 2005; Liu et al., 2004; Sun et al., 2017). The definition of "passive" and "active" is from Corti et al. (2003) and references therein. The ancient enriched lithospheric mantle (AELM) and juvenile depleted lithospheric mantle (JDLM) are from Wu et al. (2008). MTZ, mantle transition zone.

Fig. 3 (A) Structural map of the Cenozoic Jianghan Basin, illustrating the distribution of major faults and related units. Fault names: WF, Wen'ansi Fault; WcF, Wancheng Fault; ZFZ, Zibei Fault Zone; QF, Qianbei Fault; ZgF, Zhugentan Fault; TmF, Tianmenhe Fault; TF, Tonghaikou Fault; ZF, Zhanggou Fault; KF, Kaixiantai Fault; BF, Baimiao Fault; ZlF, Zhoulaozui Fault; NF, Nanmiao Fault; HF, Honghu Fault; DF, Datonghu Fault. (B) Map showing the coverage of 2-D and 3-D seismic reflection data and locations of wells. Note that only part of wells in the East Jianghan Basin are shown. See Fig. 2A for location.

Fig. 4 Stratigraphic column of the Jianghan Basin showing the key seismic horizons and systhetic well ties. The biostratigraphic data is from HBGMR (1990). The K-Ar and Ar-Ar ages are from Xu et al. (1995) and Peng et al. (2006) and shown with an error of 1 Myr.

Fig. 5 (A-B) Uninterpreted and (C-D) interpreted seismic sections across the Wancheng Fault and

Qianbei Fault, accompanied by fault activity rates (FAR; E). (F) Time-depth conversion formula constructed by checkshots from ten selected wells. Ss, Shashi Stage; Xg, Xin'gouzui Stage; Js, Jingsha Stage; Qj, Qianjiang Stage; Jh, Jinghezhen Stage. The horizons and colors of the stratigraphic units are shown in Fig. 4. See Fig. 3 for locations.

Fig. 6 (A) and (B) Field outcrop showing the conformable contact between basalt layer and overlying strata (Qianjiang Formation). (C) Photomicrograph of sample basalt (sample m-1) in the field outcrop. Pl, plagioclase; Cpx, clinopyroxene. See Fig. 3B for location.

Fig. 7 Petrophysical characteristics of basalt layers on seismic profiles (A, B and C) and in well logs (D). Wells shown by solid lines are located on the profile and wells shown by dashed line are nearby the profile. The horizons and colors of the stratigraphic units are shown in Fig. 4. From deep to shallow, the thickness of basalt layers is 13.6 m (L1), 39.8 m (L2), 18 m (L3), 8.8 m (L4), 12 m (L5) and 4.0 m (L6), respectively. Due to the detection limit of the seismic data, the fourth and sixth layers (L4 and L6) are too thin to be detected and they are show in Fig. 7B based on borehole data. The locations of the seismic profile and wells are shown in Fig. 3.

Fig. 8 Map showing the spatiotemporal variations of Fault activity rates (FAR) of the major faults and volcanic activity in the Jianghan Basin, along with two stratal thickness profiles across the West and East Jianghan basins. Fault names are as in Fig. 3A. Thickness maps showing the distribution and volume of the rift-related basalts in the Jianghan Basin. The maximum thickness of basalts erupted during the Shashi Stage is uncertain and not considered in this study, as only limited wells penetrate the basalt layers (Fig. S2A). See Figs. S1 and S3 for details of fault activity rates and the distribution and volume of basalts.

Fig. 9 (A) Chondrite-normalized rare earth element patterns and (B) primitive mantle normalized incompatible element patterns of the Jianghan basalts. Chondrite, primitive mantle, average present-day ocean island basalts (OIB) and normal type mid-ocean ridge basalts (N-MORB) data are from Sun and McDonough (1989). The data of Cenozoic basalts in the eastern SCB (Li et al., 2015b, 2016b; Liu et al., 2016; Chu et al., 2017; Zeng et al., 2017) is also plotted for comparison.

Fig. 10 (A) Sr and Nd isotope compositions of the Jianghan basalts. The data source of Cenozoic basalts in the eastern SCB is as that in Fig. 9. (B) $\varepsilon_{Nd}(t)$ vs. $\varepsilon_{Hf}(t)$ diagram for the Jianghan basalts. OIB and mid-ocean ridge basalts (MORB) data (Stracke et al., 2003, 2005) are plotted for comparison. The ranges of EM1 and EM2 are according to Zindler and Hart (1986). Reference Terrestrial Arrar ($\varepsilon_{Hf} = 1.36\varepsilon_{Nd} + 2.95$) is after Vervoort and Blichert-Toft (1999).

Fig. 11 (A) Ta*($[Ta/U]_N$) vs. Nb*($[Nb/Th]_N$) (Niu and Batiza, 1997) and (B) Nb/U versus Nb diagrams of the Jianghan basalts. The data of primitive mantle (PM), OIB and N-MORB are from Sun and McDonough (1989). The average ratios of Nb/U in MORB & OIB are from Hofmann et al. (1986). CC denotes continental crust (Rudnick and Gao, 2003). N denotes normalization to primitive mantle. The data of Cenozoic basalts in the eastern SCB is as that in Fig. 9.

Fig. 12 $[Sm/Yb]_N$ vs. $[Zr/Y]_N$ and $[Hf/Er]_N$ vs. $[Zr/Ti]_N$ diagrams showing that the late phase basalts have a smaller melting extent of asthenospheric mantle than the early phase basalts. N denotes normalization to primitive mantle.

Fig. 13 Summary of the Cenozoic tectonic evolution of the Jianghan Basin, eastern China and adjacent plates. The overlap of paleolatitudes of the northern Tethys Himalaya and southern Lhasa Block is based on Hu et al. (2016) and Meng et al. (2017) (reference point at 29ºN, 88ºE). The sedimentary changes are from Hu et al. (2016). The slab breakoff and magmatic flare-up events are from Zhu et al. (2015a). The slowdown of the Indian plate is from (Besse et al., 1984; Patriat and Achache, 1984; van Hinsbergen et al., 2011). The onset of India-Asia collision is from (Rowley, 1998; Yi et al., 2011; Meng et al., 2012; Van Hinsbergen et al., 2012; Zhu et al., 2015a; Hu et al., 2016; Ma et al., 2016). The tectonic evolution of the Tibetan Plateau is from Meng et al. (2017). The removal of the thickened lithosphere beneath the Tibetan Plateau is from Chung et al. (1998, 2005). The eastward migration of volcanic activity and eruption gap in the eastern South China Block (SCB) is from Gong and Chen (2014). The eastward migration of faulting and depocentres in the Bohai Bay Basin (BBB) is from (Qi and Yang, 2010; Suo et al., 2012, 2014; Zhao et al., 2016). The depositional break and erosion in the Subei Basin (SBB) are from (Qian, 2001; Liu et al., 2017). The dextral motion onset of the Tanlu Fault is from (Qi and Yang, 2010; Huang et al., 2015a). The sudden directional change of the Pacific plate motion is from (Sharp and Clague, 2006; Torsvik et al., 2017). The convergence rates between the Pacific and Eurasian plates are from Engebretson (1985) (dotted line) and Northrup et al. (1995) (solid line).

Fig. 14 Cartoon diagrams illustrating that eastward asthenospheric flow drove the evolution of the Jianghan Basin (cf. Niu, 2005; Liu et al., 2004; Sun et al., 2017). The horizontal extension amounts of the lithosphere are not displayed. The syn-rift sediments in each diagram represent depositions during each stage. The distribution of fluids or melts enriched in volatiles schematically represents the content of volatiles in the mantle. The ancient enriched lithospheric mantle (AELM) and juvenile depleted lithospheric mantle (JDLM) are from Wu et al. (2008). Ss, Shashi Stage; Xg, Xin'gouzui Stage; Js, Jingsha Stage; Qj, Qianjiang Stage; Jh, Jinghezhen Stage; NSGL, North-South Gravity Lineament.

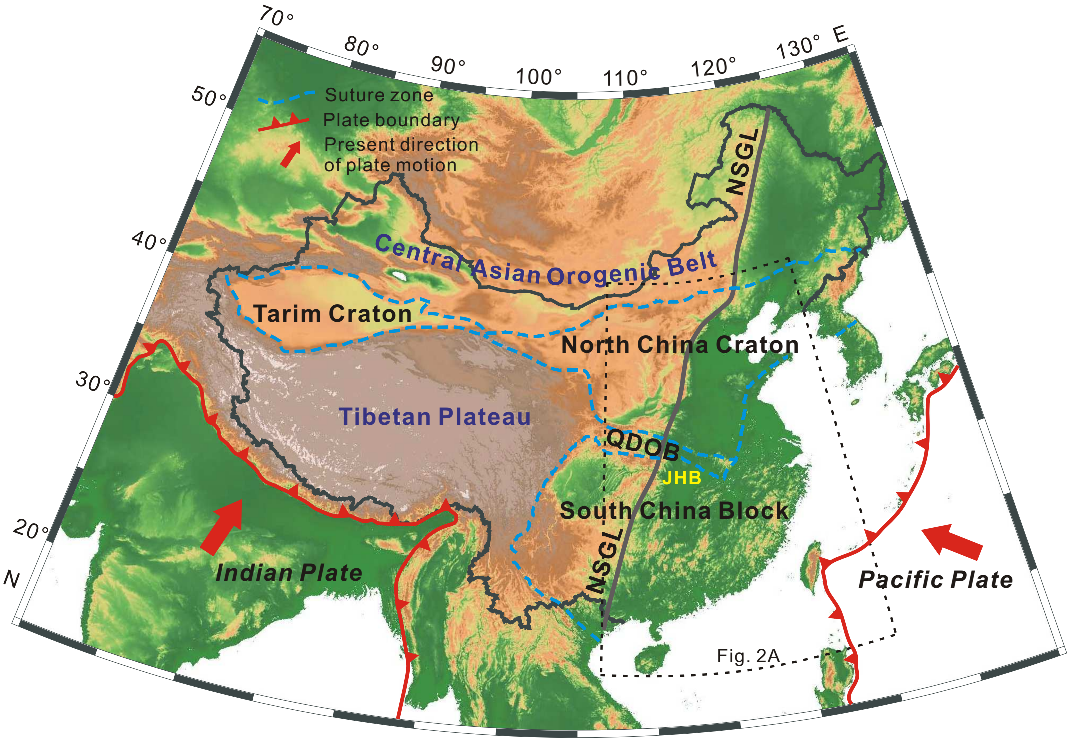
70°
80°
90°
100°
110°
120°
130°
E
50°
40°
30°
20°
N
Suture zone
Plate boundary
Present direction
of plate motion
Central Asian Orogenic Belt
NSGL
Tarim Craton
North China Craton
Tibetan Plateau
QDOB
JHB
South China Block
NSGL
Indian Plate
Pacific Plate
Fig. 2A

Fig. 1

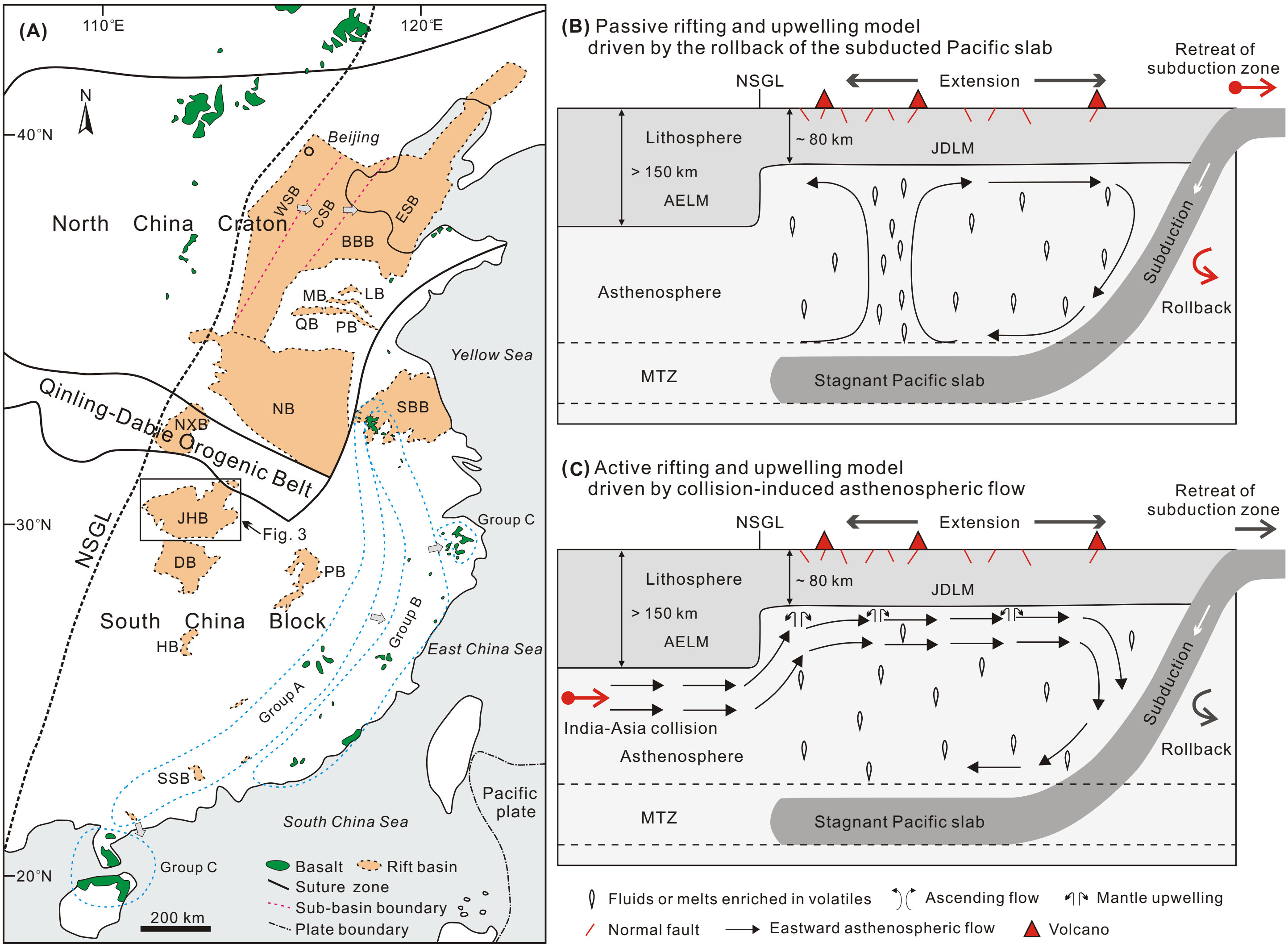
(A)
110°E
120°E
40°N
30°N
20°N
N
Beijing
North China Craton
WSB
CSB
ESB
BBB
MB
LB
QB
PB
NB
SBB
NXB
Qinling-Dabie Orogenic Belt
JHB
Fig. 3
DB
PB
NSGL
South China Block
HB
Yellow Sea
East China Sea
Group A
Group B
Group C
SSB
Group C
South China Sea
Pacific plate
Basalt
Rift basin
Suture zone
Sub-basin boundary
Plate boundary
200 km
(B) Passive rifting and upwelling model driven by the rollback of the subducted Pacific slab
NSGL
Extension
Retreat of subduction zone
Lithosphere
> 150 km
AELM
~ 80 km
JDLM
Asthenosphere
Subduction
Rollback
MTZ
Stagnant Pacific slab
(C) Active rifting and upwelling model driven by collision-induced asthenospheric flow
NSGL
Extension
Retreat of subduction zone
Lithosphere
> 150 km
AELM
~ 80 km
JDLM
India-Asia collision
Asthenosphere
Subduction
Rollback
MTZ
Stagnant Pacific slab
Fluids or melts enriched in volatiles
Ascending flow
Mantle upwelling
Normal fault
Eastward asthenospheric flow
Volcano

Fig. 2

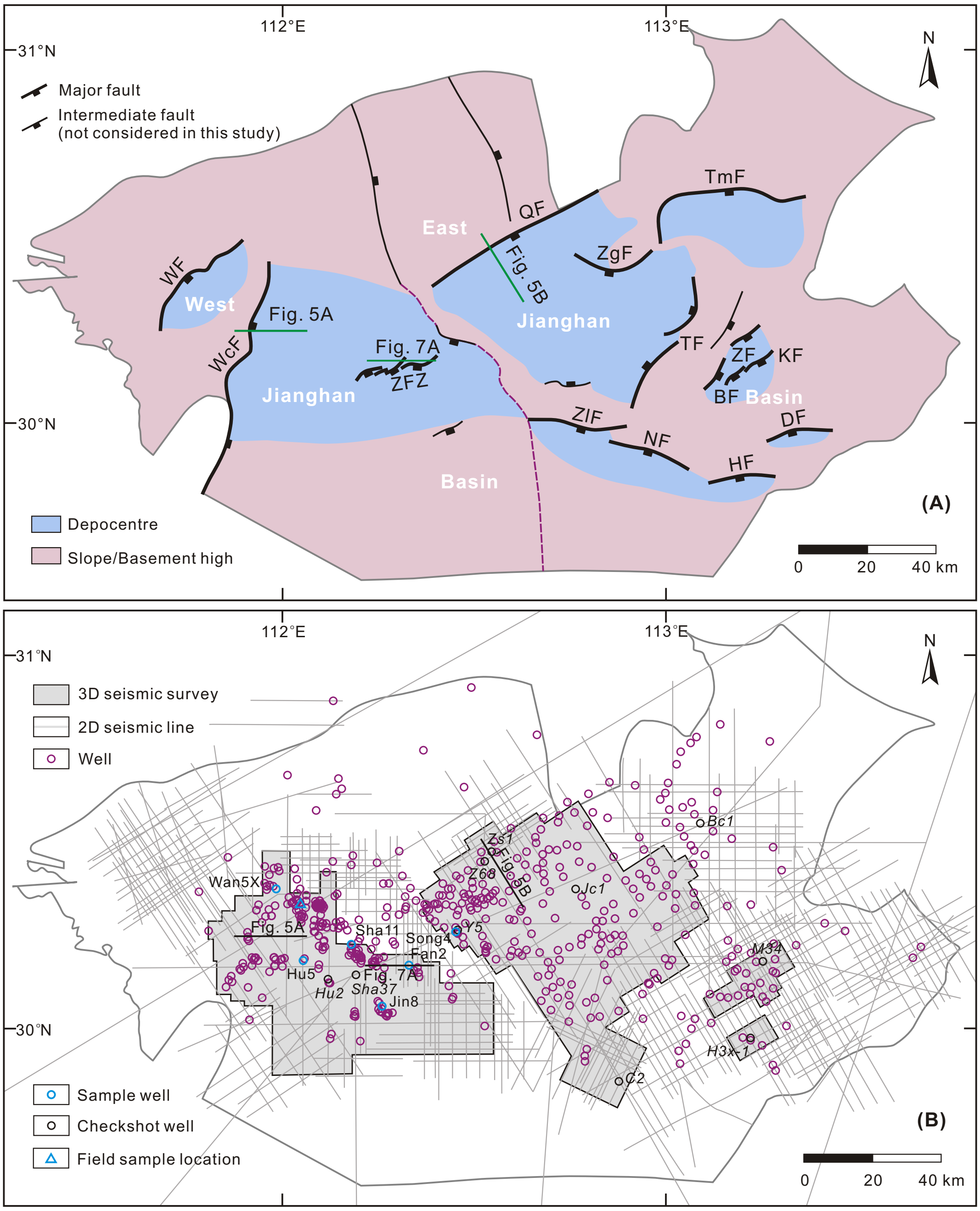

112°E
113°E
31°N
30°N
N
Major fault
Intermediate fault
(not considered in this study)
WF
West
WcF
Fig. 5A
Fig. 7A
ZFZ
Jianghan
East
QF
Fig. 5B
ZgF
TmF
Jianghan
TF
ZF
KF
BF
Basin
ZlF
NF
DF
HF
Basin
Depocentre
Slope/Basement high
(A)
0
20
40 km
3D seismic survey
2D seismic line
Well
Wan5X
Fig. 5A
Hu5
Hu2
Sha11
Song4
Fan2
Fig. 7A
Sha37
Jin8
Zs1
Z68
Fig. 5B
Y5
Jc1
Bc1
M34
H3x-1
C2
Sample well
Checkshot well
Field sample location
(B)

Fig. 3

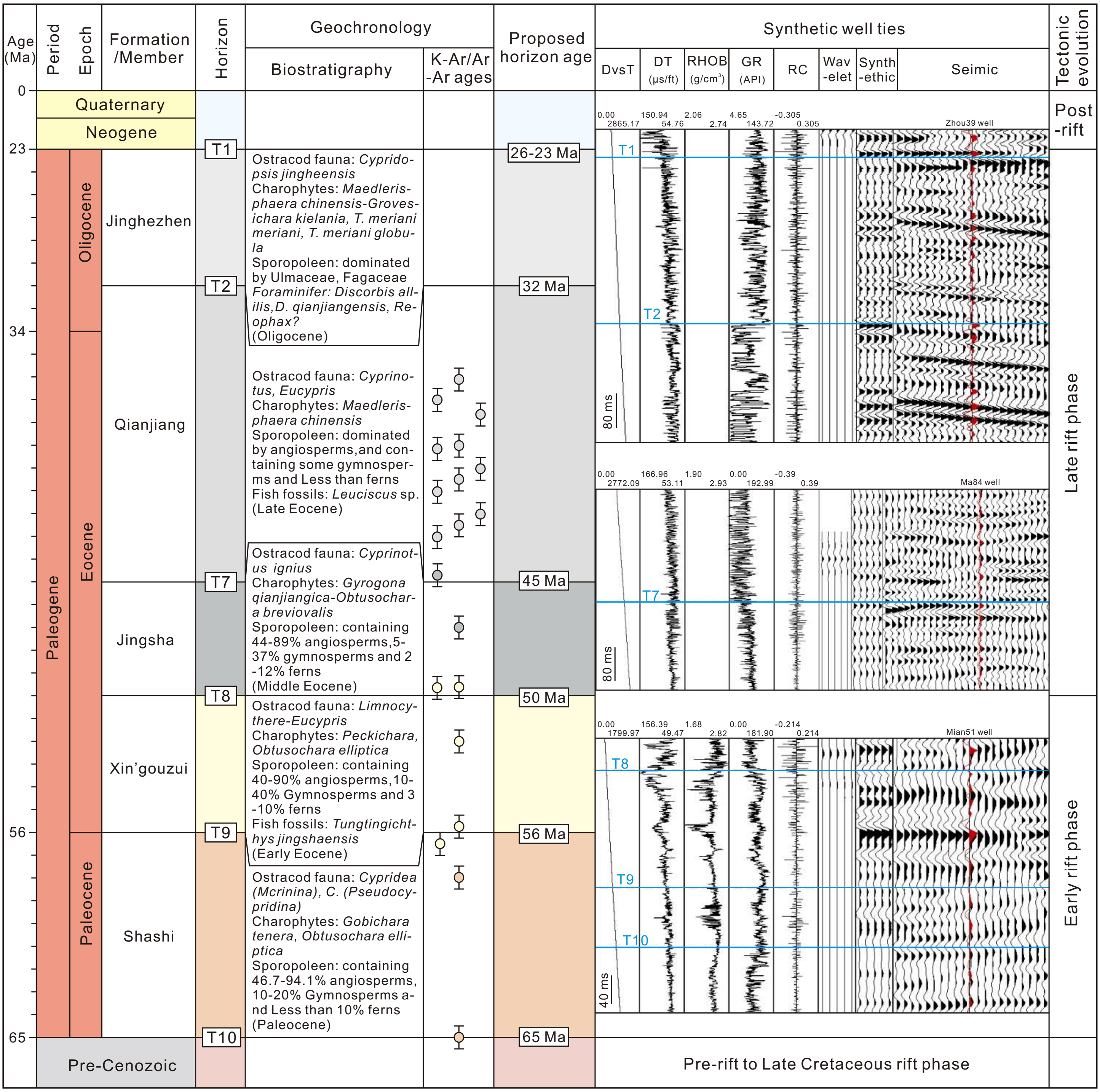

Age (Ma)
Period
Epoch
Formation /Member
Horizon
Geochronology
Biostratigraphy
K-Ar/Ar -Ar ages
Proposed horizon age
Synthetic well ties
DvsT
DT (μs/ft)
RHOB (g/cm³)
GR (API)
RC
Wav -elet
Synth -ethic
Seimic
Tectonic evolution
0
23
34
56
65
Quaternary
Neogene
Paleogene
Oligocene
Eocene
Paleocene
Pre-Cenozoic
Jinghezhen
Qianjiang
Jingsha
Xin'gouzui
Shashi
T1
T2
T7
T8
T9
T10
Ostracod fauna: Cypridopsis jingheensis
Charophytes: Maedlerisphaera chinensis-Grovesichara kielania, T. meriani meriani, T. meriani globula
Sporopoleen: dominated by Ulmaceae, Fagaceae
Foraminifer: Discorbis allilis, D. qianjiangensis, Reophax?
(Oligocene)
Ostracod fauna: Cyprinotus, Eucypris
Charophytes: Maedlerisphaera chinensis
Sporopoleen: dominated by angiosperms, and containing some gymnosperms and Less than ferns
Fish fossils: Leuciscus sp.
(Late Eocene)
Ostracod fauna: Cyprinotus ignius
Charophytes: Gyrogona qianjiangica-Obtusochara breviovalis
Sporopoleen: containing 44-89% angiosperms, 5-37% gymnosperms and 2-12% ferns
(Middle Eocene)
Ostracod fauna: Limnocythere-Eucypris
Charophytes: Peckichara, Obtusochara elliptica
Sporopoleen: containing 40-90% angiosperms, 10-40% Gymnosperms and 3-10% ferns
Fish fossils: Tungtingichthys jingshaensis
(Early Eocene)
Ostracod fauna: Cypridea (Mcrinina), C. (Pseudocypridina)
Charophytes: Gobichara tenera, Obtusochara elliptica
Sporopoleen: containing 46.7-94.1% angiosperms, 10-20% Gymnosperms and Less than 10% ferns
(Paleocene)
26-23 Ma
32 Ma
45 Ma
50 Ma
56 Ma
65 Ma
Zhou39 well
Ma84 well
Mian51 well
80 ms
80 ms
40 ms
Post -rift
Late rift phase
Early rift phase
Pre-rift to Late Cretaceous rift phase

Fig. 4

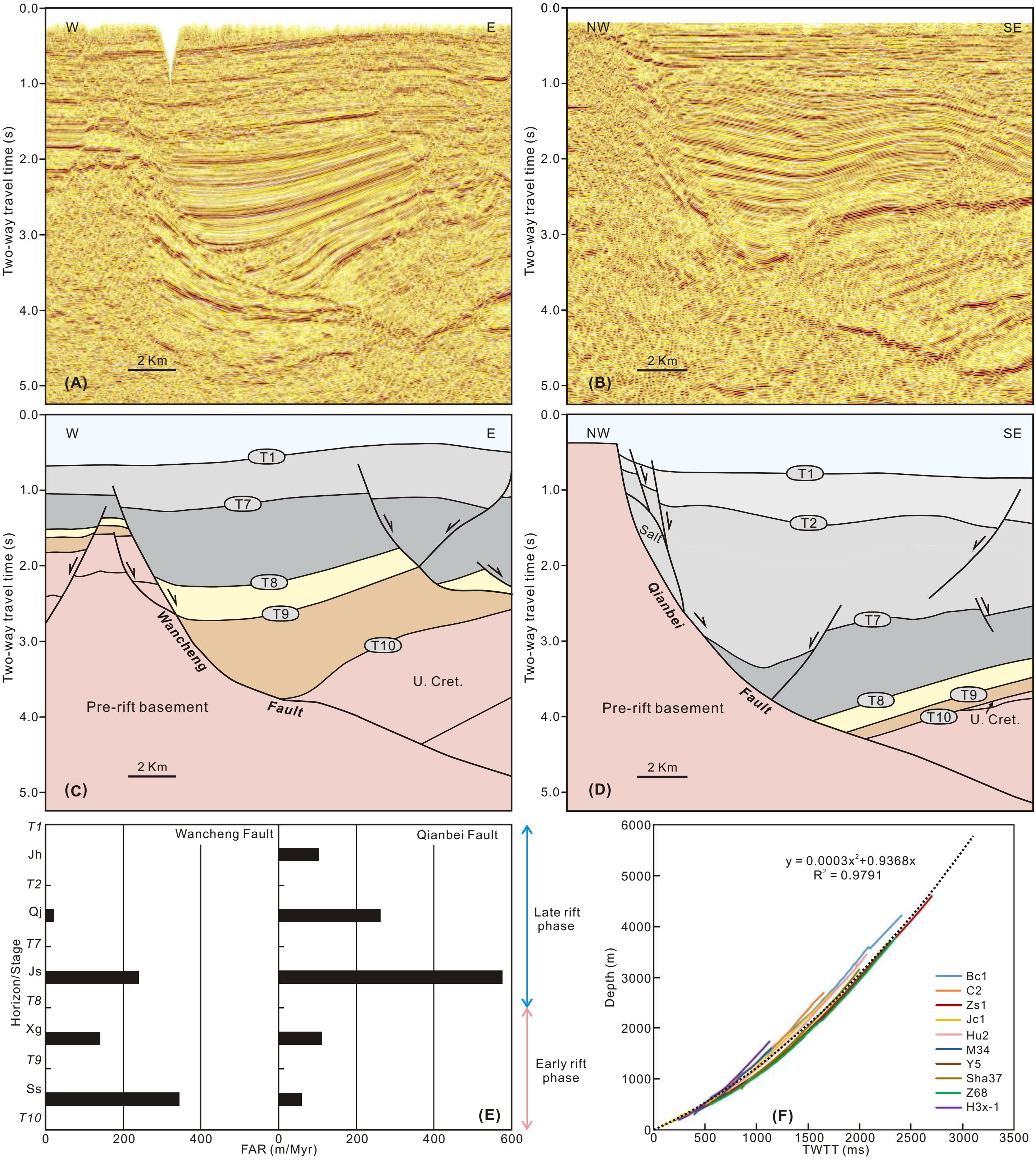

W
E
NW
SE
Two-way travel time (s)
2 Km
(A)
(B)
T1
T2
T7
T8
T9
T10
Salt
Wancheng
Fault
Qianbei
Fault
U. Cret.
Pre-rift basement
(C)
(D)
Wancheng Fault
Qianbei Fault
Horizon/Stage
Jh
Qj
Js
Xg
Ss
Late rift phase
Early rift phase
FAR (m/Myr)
(E)
y = 0.0003x²+0.9368x
R² = 0.9791
Depth (m)
TWTT (ms)
Bc1
C2
Zs1
Jc1
Hu2
M34
Y5
Sha37
Z68
H3x-1
(F)

Fig. 5


(A)
Sediments
Fig. 6B
Basalt
Fig. 6C
2 m
(B)
Mudstone
Basalt
10 cm
(C)
Cpx
Pl
0.2 mm

Fig. 6

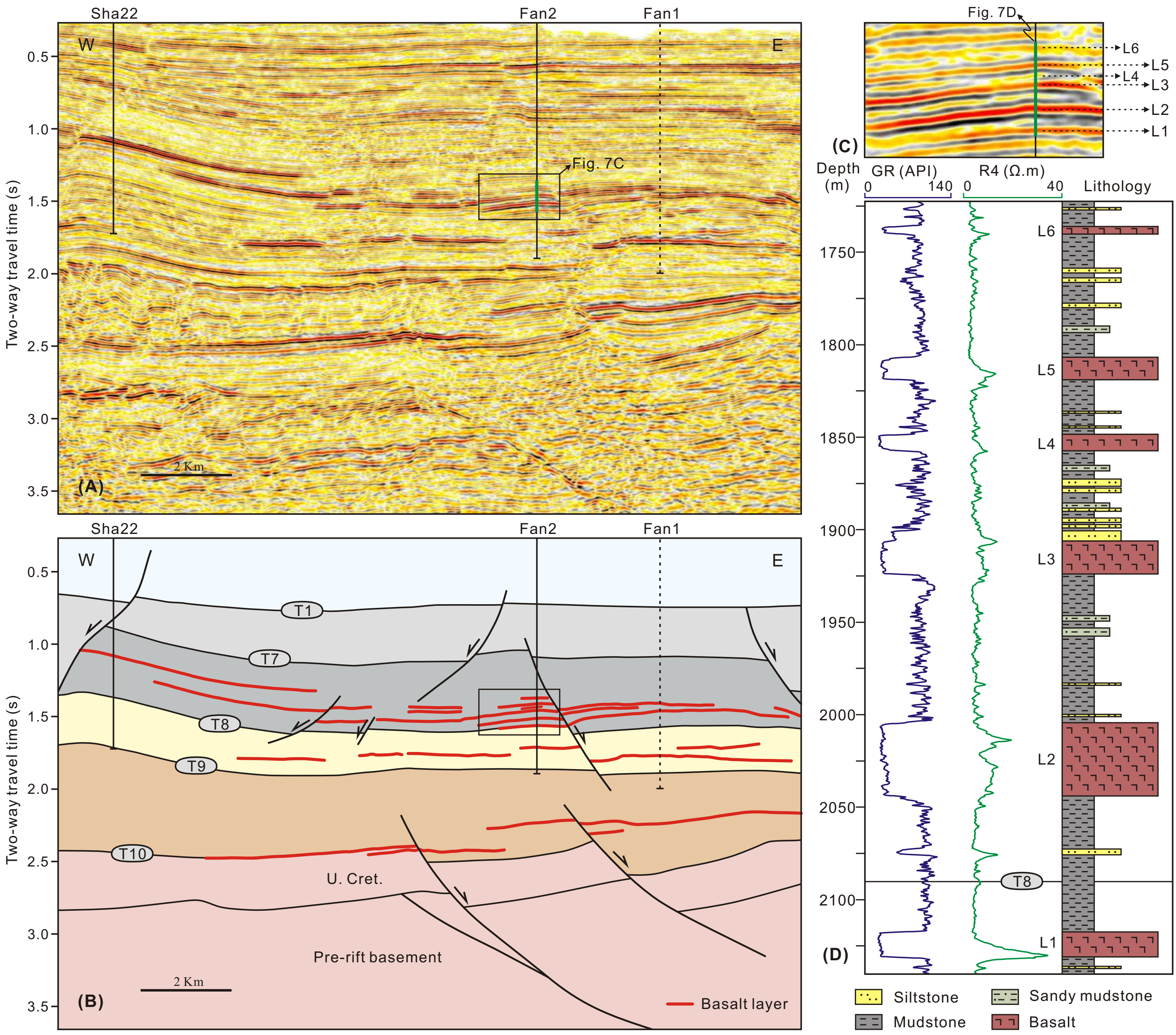

Sha22
Fan2
Fan1
W
E
Fig. 7C
Two-way travel time (s)
2 Km
(A)
T1
T7
T8
T9
T10
U. Cret.
Pre-rift basement
(B)
Basalt layer
Fig. 7D
L6
L5
L4
L3
L2
L1
(C)
Depth (m)
GR (API)
R4 (Ω.m)
Lithology
(D)
Siltstone
Sandy mudstone
Mudstone
Basalt

Fig. 7

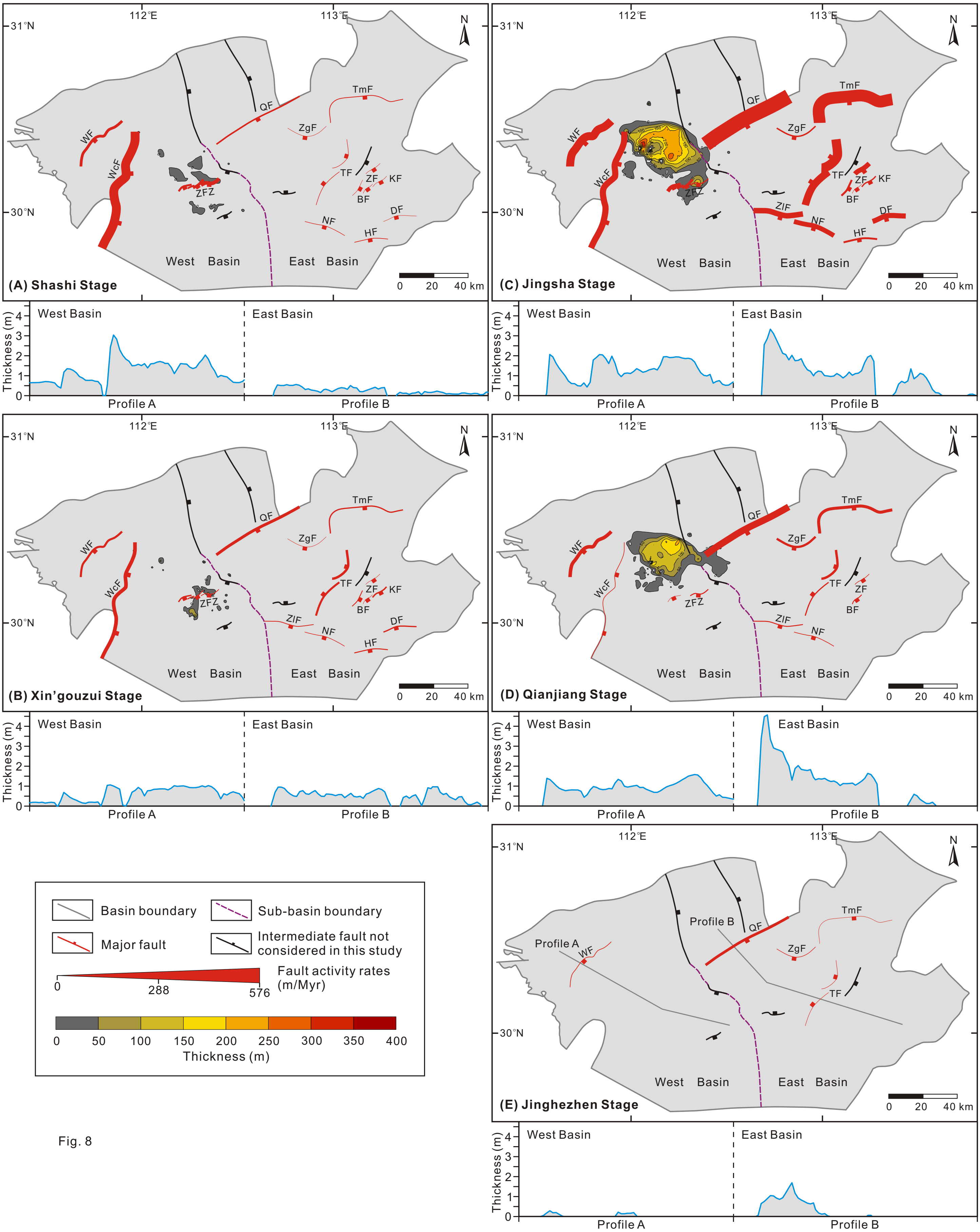

(A) Shashi Stage
(B) Xin'gouzui Stage
(C) Jingsha Stage
(D) Qianjiang Stage
(E) Jinghezhen Stage
112°E
113°E
31°N
30°N
N
West Basin
East Basin
QF
TmF
ZgF
WF
WcF
ZFZ
TF
ZF
KF
BF
DF
NF
HF
ZIF
Profile A
Profile B
0 20 40 km
Thickness (m)
Basin boundary
Sub-basin boundary
Major fault
Intermediate fault not considered in this study
Fault activity rates (m/Myr)
0
288
576
0 50 100 150 200 250 300 350 400
Thickness (m)

Fig. 8

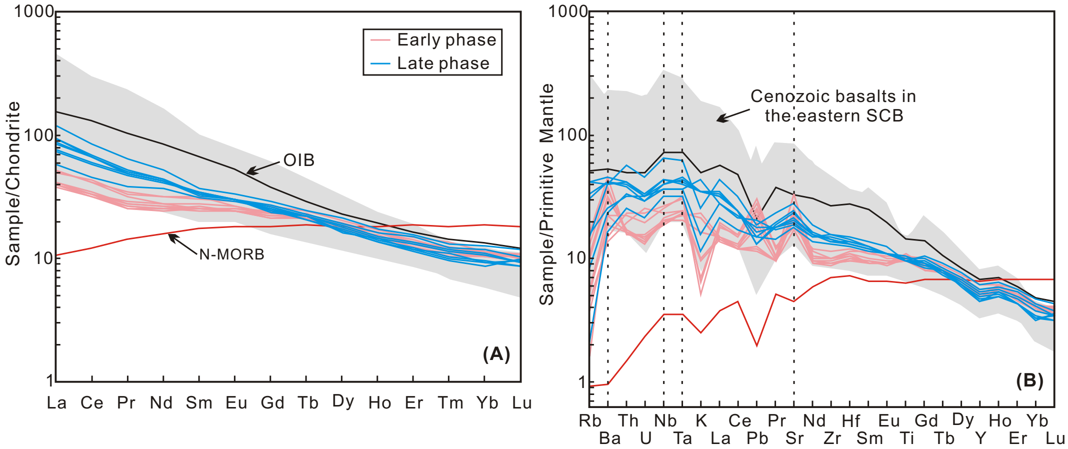

Early phase
Late phase
OIB
N-MORB
(A)
Sample/Chondrite
1000
100
10
1
La Ce Pr Nd Sm Eu Gd Tb Dy Ho Er Tm Yb Lu
Cenozoic basalts in the eastern SCB
(B)
Sample/Primitive Mantle
Rb Ba Th U Nb Ta K La Ce Pb Pr Sr Nd Zr Hf Sm Eu Ti Gd Tb Dy Y Ho Er Yb Lu

Fig. 9

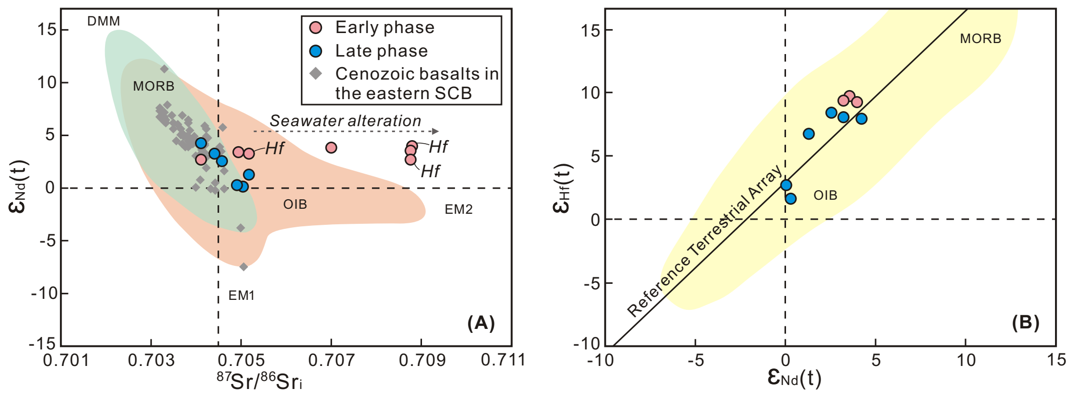
DMM
MORB
Early phase
Late phase
Cenozoic basalts in the eastern SCB
Seawater alteration
Hf
Hf
Hf
OIB
EM2
EM1
(A)
εNd(t)
87Sr/86Sri
0.701
0.703
0.705
0.707
0.709
0.711
15
10
5
0
-5
-10
-15
MORB
OIB
Reference Terrestrial Array
(B)
εHf(t)
εNd(t)
-10
-5
0
5
10
15

Fig. 10

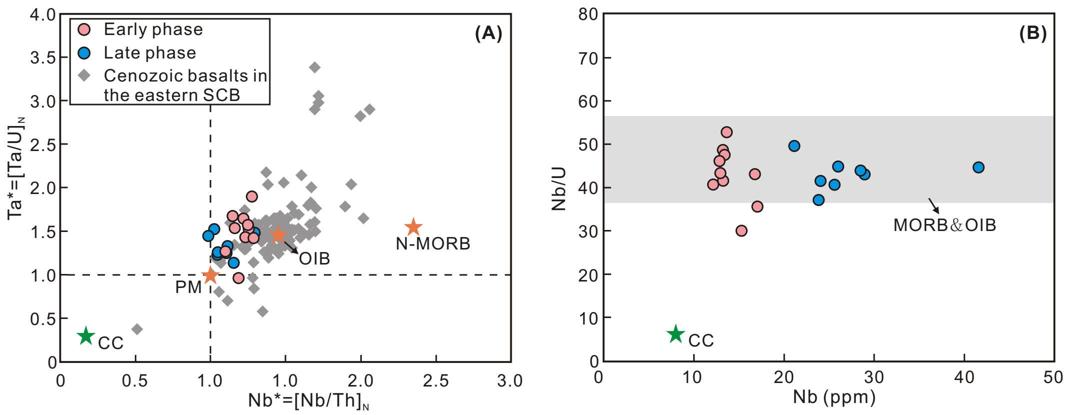

(A)
Early phase
Late phase
Cenozoic basalts in the eastern SCB
Ta*=[Ta/U]N
Nb*=[Nb/Th]N
OIB
N-MORB
PM
CC
4.0
3.5
3.0
2.5
2.0
1.5
1.0
0.5
0
0.5
1.0
2.0
2.5
3.0
(B)
Nb/U
Nb (ppm)
MORB&OIB
CC
80
70
60
50
40
30
20
10
0

Fig. 11

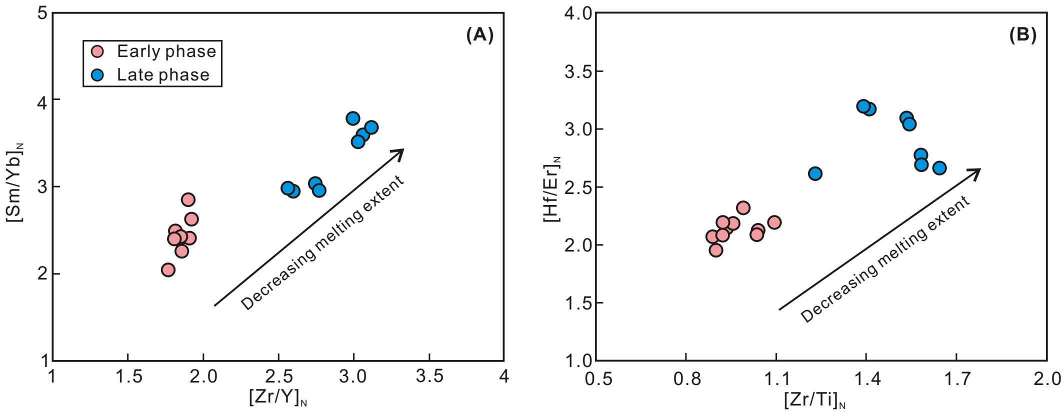

(A)
Early phase
Late phase
Decreasing melting extent
[Sm/Yb]N
[Zr/Y]N
(B)
Decreasing melting extent
[Hf/Er]N
[Zr/Ti]N

Fig. 12

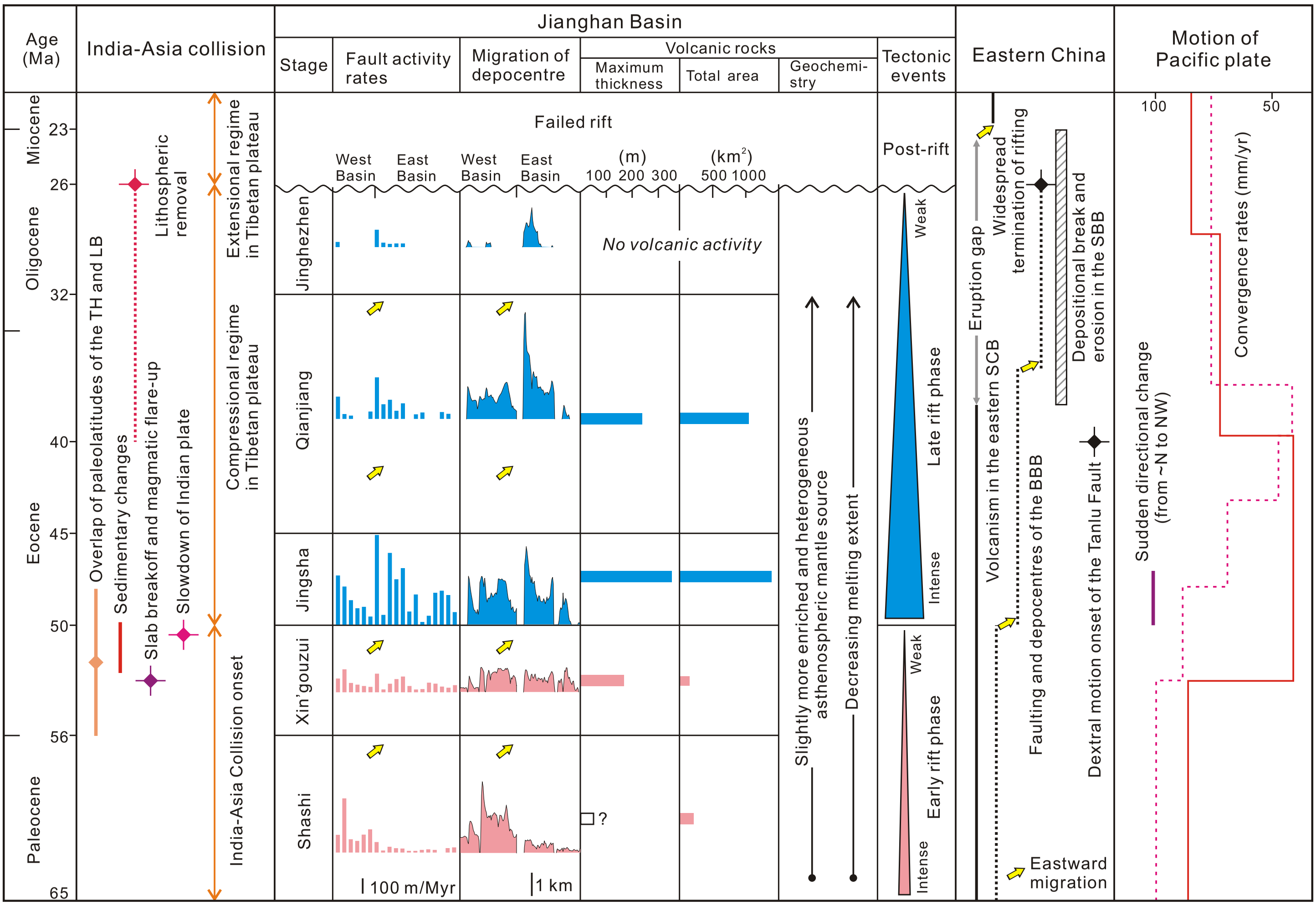

Age (Ma)
India-Asia collision
Jianghan Basin
Stage
Fault activity rates
Migration of depocentre
Volcanic rocks
Maximum thickness
Total area
Geochemistry
Tectonic events
Eastern China
Motion of Pacific plate
Miocene
Oligocene
Eocene
Paleocene
23
26
32
40
45
50
56
65
Overlap of paleolatitudes of the TH and LB
Sedimentary changes
Slab breakoff and magmatic flare-up
Slowdown of Indian plate
Lithospheric removal
India-Asia Collision onset
Compressional regime in Tibetan plateau
Extensional regime in Tibetan plateau
Failed rift
West Basin
East Basin
(m)
100 200 300
(km²)
500 1000
Jinghezhen
Qianjiang
Jingsha
Xin'gouzui
Shashi
No volcanic activity
100 m/Myr
1 km
Slightly more enriched and heterogeneous asthenospheric mantle source
Decreasing melting extent
Post-rift
Weak
Late rift phase
Intense
Early rift phase
Eruption gap
Widespread termination of rifting
Volcanism in the eastern SCB
Faulting and depocentres of the BBB
Depositional break and erosion in the SBB
Dextral motion onset of the Tanlu Fault
Eastward migration
100
50
Convergence rates (mm/yr)
Sudden directional change (from ~N to NW)

Fig.13

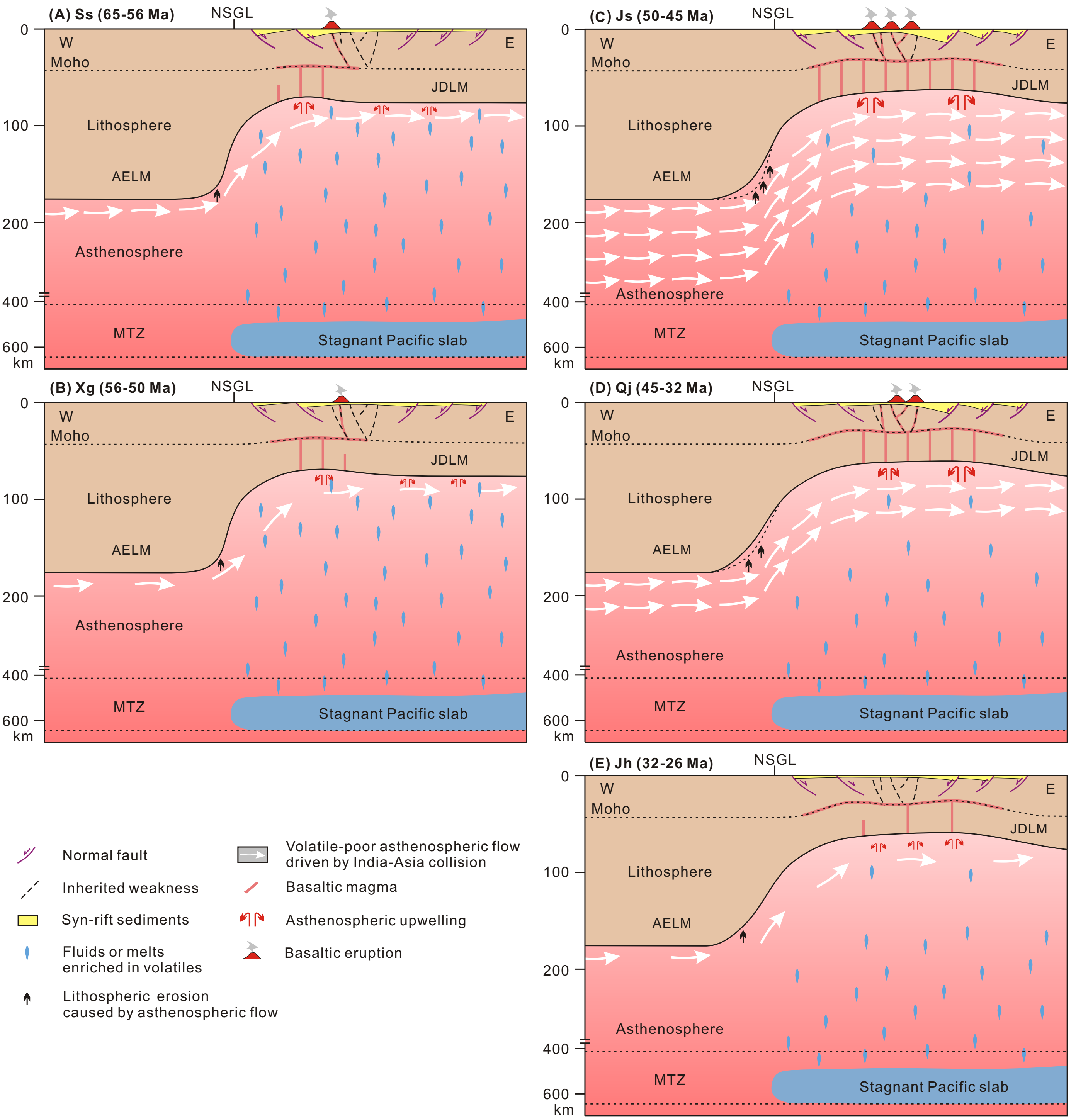

(A) Ss (65-56 Ma)
NSGL
0
W
E
Moho
JDLM
100
Lithosphere
AELM
200
Asthenosphere
400
MTZ
600
km
Stagnant Pacific slab
(B) Xg (56-50 Ma)
NSGL
(C) Js (50-45 Ma)
(D) Qj (45-32 Ma)
(E) Jh (32-26 Ma)
Normal fault
Inherited weakness
Syn-rift sediments
Fluids or melts enriched in volatiles
Lithospheric erosion caused by asthenospheric flow
Volatile-poor asthenospheric flow driven by India-Asia collision
Basaltic magma
Asthenospheric upwelling
Basaltic eruption

Fig. 14